## ORIGINAL RESEARCH

Human Intestinal Enteroids With Inducible Neurogenin-3 Expression as a Novel Model of Gut Hormone Secretion

Alexandra L. Chang-Graham,[1,*] Heather A. Danhof,[1,*] Melinda A. Engevik,[2,3,*]
Catherine Tomaro-Duchesneau,[1,*] Umesh C. Karandikar,[1] Mary K. Estes,[1,4]
James Versalovic,[2,3] Robert A. Britton,[1] and Joseph M. Hyser[1]

[1]Department of Molecular Virology and Microbiology, [2]Department of Pathology and Immunology, [4]Department of Medicine,
Gastroenterology and Hepatology, Baylor College of Medicine, Houston, Texas; [3]Department of Pathology, Texas Children's
Hospital, Houston, Texas
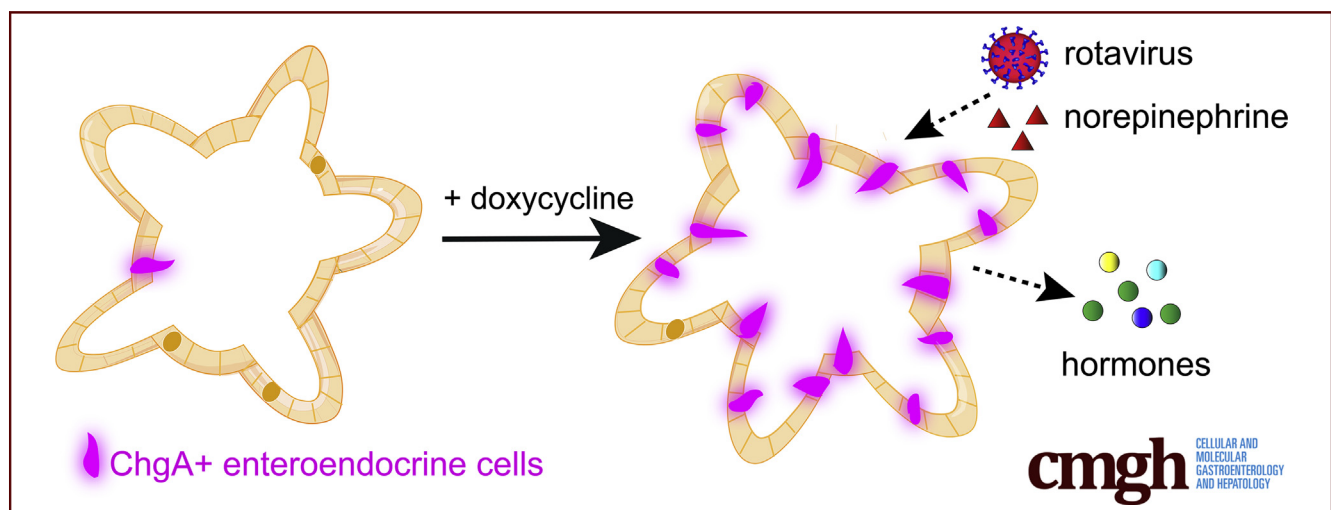
SUMMARY

Enteroendocrine cells have low abundance but exert widespread effects on gastrointestinal physiology. We engineered human intestinal enteroids with inducible expression of neurogenin-3, resulting in increased enteroendocrine cells and facilitating investigations of host responses to the dynamic intestinal environment.

BACKGROUND & AIMS: Enteroendocrine cells (EECs) are specialized epithelial cells that produce molecules vital for intestinal homeostasis, but because of their limited numbers, in-depth functional studies have remained challenging. Human intestinal enteroids (HIEs) that are derived from intestinal crypt stem cells are biologically relevant in an in vitro model of the intestinal epithelium. HIEs contain all intestinal epithelial cell types; however, similar to the intestine, HIEs spontaneously produce few EECs, which limits their study.

METHODS: To increase the number of EECs in HIEs, we used lentivirus transduction to stably engineer jejunal HIEs with doxycycline-inducible expression of neurogenin-3 (*NGN3*), a transcription factor that drives EEC differentiation (tet*NGN3*-HIEs). We examined the impact of *NGN3* induction on EECs by quantifying the increase in the enterochromaffin cells and other EEC subtypes. We functionally assessed secretion of serotonin and EEC hormones in response to norepinephrine and rotavirus infection.

RESULTS: Treating tet*NGN3*-HIEs with doxycycline induced a dose-dependent increase of chromogranin A (ChgA)-positive and serotonin-positive cells, showing increased enterochromaffin cell differentiation. Despite increased ChgA-positive cells, other differentiated cell types of the epithelium remained largely unchanged by gene expression and immunostaining. RNA sequencing of doxycycline-induced tet*NGN3*-HIEs identified increased expression of key hormones and enzymes associated with several other EEC subtypes. Doxycycline-induced tet*NGN3*-HIEs secreted serotonin, monocyte chemoattractant protein-1, glucose-dependent insulinotropic peptide, peptide YY, and ghrelin in response to norepinephrine and rotavirus infection, further supporting the presence of multiple EEC types.

CONCLUSIONS: We have combined HIEs and inducible-*NGN3* expression to establish a flexible in vitro model system for functional studies of EECs in enteroids and advance the molecular and physiological investigation of EECs. *(Cell Mol Gastroenterol Hepatol 2019;8:209–229; https://doi.org/10.1016/j.jcmgh.2019.04.010)*

Keywords: Enteroendocrine Cell; Enteroid; Serotonin.

See editorial on page 291.

The gastrointestinal (GI) epithelium is the largest sensory interface between the host and environment and must both detect and communicate luminal contents to the host.[1] The GI lumen is a complex mixture of dietary nutrients and their breakdown products, microorganisms, and their metabolites, as well as irritants, toxins, and drugs. Microorganisms in particular create a dynamic ecosystem in the GI lumen with both beneficial and detrimental effects. For example, the gut microbiome is important for degradation of complex carbohydrates and polysaccharides into short-chain fatty acids such as acetate, butyrate, and propionate, which can be used as nutrients by the host or other microbes. Short-chain fatty acids also modulate a variety of important physiological effects such as inflammation and gut motility.[2] By contrast, pathogenic microorganisms invade the epithelium or produce toxins that threaten the GI epithelial barrier and thus necessitate activation of host defenses. Therefore, integrating signals from luminal stimuli to the host for coordinated and appropriate physiological responses is complex, which has complicated efforts to study the molecular mechanisms governing these processes.

Microbiome-to-epithelium communication is multifaceted and includes receptors on various cell types, including enterocytes, goblet cells, Paneth cells, and stem cells. Recent evidence has shown that enteroendocrine cells are one of the most important mediators of communication between the GI lumen and host.[3] Enteroendocrine cells (EECs) are a rare cell lineage found throughout the length of the GI tract (<1% of GI epithelial cells), yet they have a significant impact on human physiology.[4–6] In response to host, microbial, and environmental stimuli, subtypes of EECs synthesize and secrete hormones including gastrin (G cells), somatostatin (D cells), enteroglucagon/peptide YY (PYY), glucagon-like peptide 1 (GLP-1) (L cells), neurotensin (N cells), pro-γ-melanocyte-stimulating hormone cells, and serotonin (enterochromaffin cells).[7–9] The broad array of enteroendocrine cell types reflects the diversity of critical physiological functions including the coordination of both local and systemic responses by the endocrine and nervous systems to the stimuli present in the lumen. Enterochromaffin cells are the most common EEC subtype, comprising ∼40% of EECs. These cells synthesize and secrete the neurotransmitter serotonin in response to various physiological stimuli, including microbial metabolites, irritants, toxins, and infection.[10–12] Given the importance of serotonin in mammalian physiology and greater abundance among EECs, many studies focus on enterochromaffin cells, but owing in part to their rarity, how other EEC subtypes function in the context of the gut environment remains less well studied.

Studying the interaction of EECs and stimuli in the GI lumen has been challenging because of the limited number of these cells in the intestinal epithelium and the lack of appropriate non–cancer-derived in vitro models. Generation of enteroids is a recent technology that has revolutionized the study of intestinal epithelial cells. They have been generated from several mammalian hosts, including mice and human beings, and recapitulate the GI physiology of the donor species.[13–16] This complex epithelial culture system is derived from adult stem cells isolated from intestinal tissue or biopsy samples that can be maintained and expanded in culture as an in vitro model system.[13–15,17–21] Thus, enteroids offer a promising new tool to study nontransformed, noncancerous, human EECs in an in vitro culture system.[17]

Previous studies have established that neurogenin 3 (Ngn3) is a key transcription factor for EEC differentiation.[22–36] Consistent with the role of Ngn3 in EEC fate, overexpression of *NGN3* in multiple systems has been shown to increase EEC numbers.[37,38] In vitro, adenoviral-based *NGN3* overexpression in neonatal mouse jejunal intestinal spheres induced a 3-fold increase in the number of chromogranin A (ChgA)-positive EECs.[39] In human intestinal organoids (HIOs) derived from pluripotent stem cells, overexpression of *NGN3* by an adenoviral vector or tetracycline-inducible lentiviral vector also increased ChgA-positive EECs.[29,40] In this study, we generated a new model system using jejunal human intestinal enteroids (HIEs) engineered to overexpress *NGN3* from a tetracycline-inducible promoter (tet*NGN3*) to drive EEC differentiation. These tet*NGN3*-HIEs show a doxycycline dose-dependent increase in ChgA expression in both 3-dimensional (3D) culture and as 2-dimensional (2D) monolayers, as well as up-regulation of markers for multiple EEC subtypes, including enterochromaffin cells, L cells, and K cells. In response to microbial and host stimuli, these induced EECs secreted serotonin, monocyte chemoattractant protein-1 (MCP-1), glucose-dependent insulinotropic peptide (GIP), PYY, and ghrelin. Thus, tet*NGN3*-HIEs are a new and physiologically relevant model system to study EEC-based communication pathways in response to both microbial and host stimuli.

Results

Creation and Propagation of Inducible tetNGN3-HIEs

Because host–microbe interactions via EECs has a profound impact on host physiology, we sought to develop a new
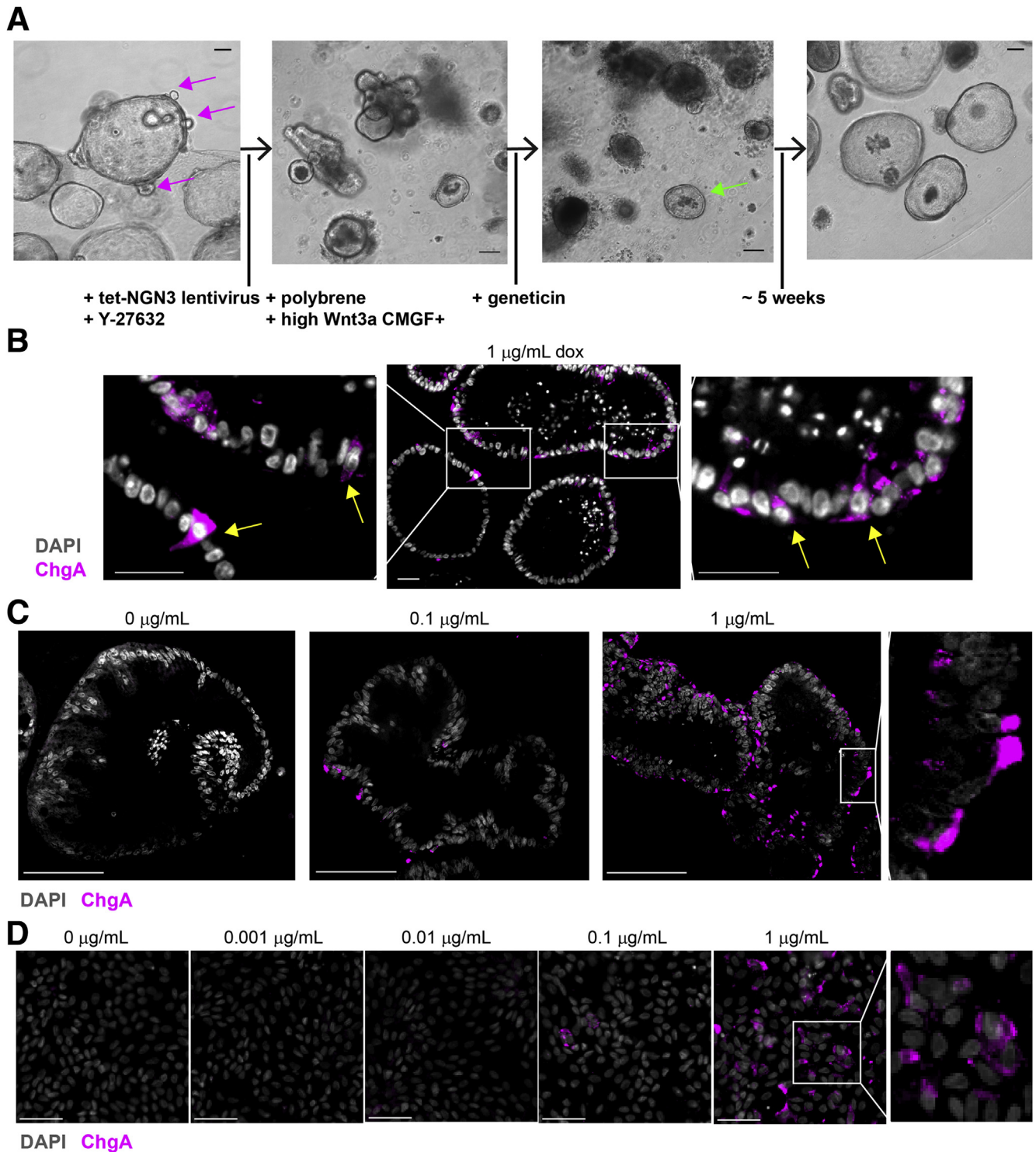
Most current article

Figure 1. (*A*) **Production pipeline for creating tet*NGN3*-HIEs using lentivirus transduction.** Jejunum HIEs grown in hW-CMGF+ media increases stem cells, evidenced by cysts and crypt buds (*pink arrows*), followed by inoculation with lentivirus. Reseeding the HIEs in Matrigel is followed by geneticin selection for approximately 5 weeks, so that only HIEs with tet*NGN3* construct survive (*green arrow*). *Scale bar*: 100 μm. Images were acquired using a 10× Plan Fluor (numerical aperture, 0.3) phase-contrast objective on an inverted Nikon TiE microscope with an ORCA-Flash 4.0 sCMOS camera and Nikon Elements software. (*B–D*) Doxycycline induces enterochromaffin marker ChgA expression in tet*NGN3*-HIEs. Tet*NGN3*-HIEs were fixed and stained for ChgA (Alexa Fluor 488, pink) to mark enterochromaffin cells and counterstained with DAPI (gray). (*B*) 3D tet*NGN3*-HIEs were differentiated for 4 days with 1 μg/mL doxycycline. *Scale bars*: 25 μm. ChgA-positive cells (*inset*) were observed (*yellow arrows*). (*C* and *D*) tet*NGN3*-HIEs as (*C*) 3D cultures and (*D*) flat monolayers were differentiated for 4 days with 0, 0.1, and 1 μg/mL doxycycline and also 0.01 and 0.001 μg/mL doxycycline in flat monolayers. 3D culture images were acquired using a 20× Plan Apo (NA, 0.75) DIC objective on an upright Nikon Eclipse 90i microscope with a Photometrics CoolSNAP HQ2 camera and Nikon Elements software. *Scale bar*: 100 μm. Flat monolayer images were acquired using a 20× Plan Apo (NA, 0.75) DIC objective on an inverted Nikon TiE microscope with an ORCA-Flash 4.0 sCMOS camera and Nikon Elements software. *Scale bar*: 50 μm.

model for screening, identification, and testing of microbe-induced EEC responses. Because of the low abundance of EECs within intestinal tissue and HIEs, we aimed to increase EEC abundance through inducible overexpression of *NGN3* using lentivirus transduction to introduce a doxycycline-inducible NGN3 expression cassette into an HIE.[41,42] In preparation for transduction, jejunal HIEs were grown in high Wnt complete media with growth factors (hW-CMGF+) to enrich the stem cell population, which was evidenced by the majority of HIEs showing a cystic morphology with multiple small buds (Figure 1*A*, left panel). Growth in high Wnt media was important for increasing the success rate of the transduction. After lentivirus transduction, geneticin selection initially increased sloughing of dead cells from the HIEs, and full selection of transduced tet*NGN3*-HIEs occurred after ∼5 weeks (Figure 1*A*, right panel).

To confirm the ability of *NGN3* to drive EEC differentiation we used immunofluorescence staining for ChgA as a marker of endocrine cells, which often are used to assess increases in EEC numbers upon *NGN3* overexpression.[29,39,40] First, the number of ChgA-positive cells present in the tet*NGN3*-HIEs

after induction with 1 *μ*g/mL doxycycline was assessed (Figure 1*B*; see antibodies in Table 1). In paraffin-embedded slices of 3D tet*NGN3*-HIE cultures, we observed abundant ChgA-positive cells in both apical and basolateral areas of cells (Figure 1*B*). In contrast to the doxycycline-induced tet*NGN3*-HIEs, very few ChgA-positive cells were observed in the absence of doxycycline (Figure 1*C*, left panel). However, induction of tet*NGN3* increased the number of ChgA-positive cells in a doxycycline dose-dependent manner (Figure 1*C*). A similar doxycycline dose-dependent increase in ChgA-positive cells was observed in 2D flat monolayers (Figure 1*D*). Of note, the ChgA-positive cells in both 3D and 2D formats showed the polygonal cell shape typically associated with enterochromaffin cells.[43]

By using image analysis software, we quantified the abundance of ChgA-positive cells from the different doxycycline-induction conditions described earlier. In the absence of doxycycline, both 3D and monolayer tet*NGN3*-HIEs showed few to no ChgA-positive cells. In contrast, addition of 0.1 *μ*g/mL and 1 *μ*g/mL doxycycline to 3D tet*NGN3*-HIEs resulted in a dose-dependent increase in the
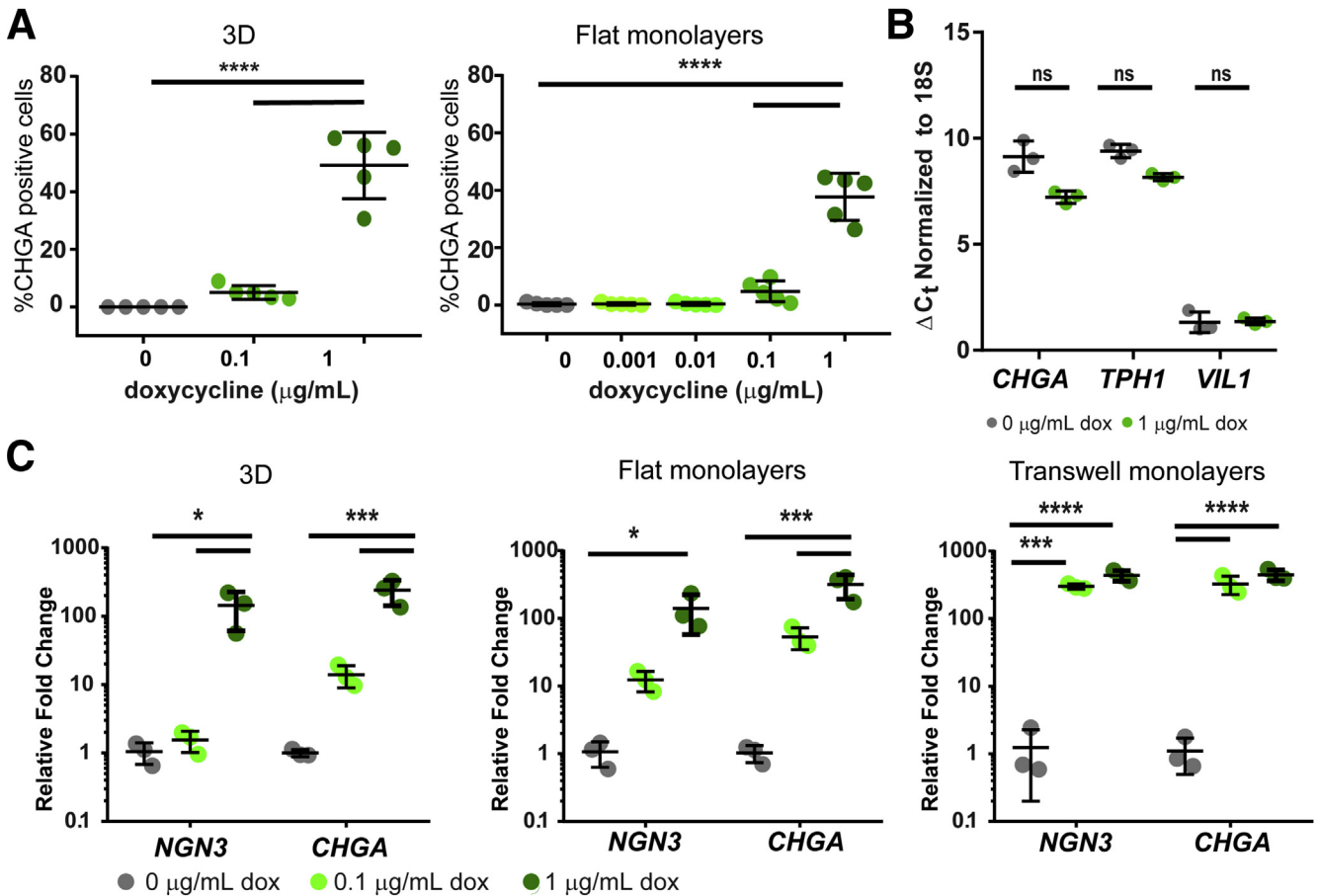

Figure 2. Doxycycline induces enteroendocrine cell lineage in tet*NGN3*-HIEs. (*A*) Increased doxycycline concentration increases the percentage of ChgA-positive cells in differentiated tet*NGN3*-HIE 3D cultures and flat monolayers. Images were analyzed with Nikon elements software with 5 images per condition with an average of 220 nuclei per image in 3D cultures and 1400 nuclei per image in flat monolayers. n = 2 biological replicates. (*B*) qPCR of *CHGA*, *TPH1* (tryptophan hydrolase-1), and *VIL1* mRNA transcripts of parental jejunum 3D enteroids were treated with 0 or 1 *μ*g/mL doxycycline and normalized to 18S mRNA. n = 3 biological replicates. (*C*) qPCR of *NGN3* and *CHGA* mRNA transcripts normalized to 18S mRNA transcripts in tet*NGN3* 3D cultures, flat monolayers, and Transwell monolayers. n = 3 biological replicates. ΔCt represents the delta (change in) CT relative to GAPDH. *$P < .05$, ***$P < .001$, and ****$P < .0001$.

Table 1. Antibodies Used in This Study

Antibody type	Target	Species	Company	Catalog	Dilution
Primary	Muc2	Mouse	Santa Cruz (Dallas, TX)	sc-515032	1:200
Primary	Sucrase isomaltase	Mouse	Santa Cruz	sc-393470	1:100
Primary	Sodium-glucose transporter 1/SLC5A1	Rabbit	Novus Biologicals (Centennial, CO)	NBP-238748	1:100
Primary	Chromogranin A	Rabbit	Novus Biologicals	NBP-253140	1:500
Primary	Serotonin	Goat	Immunostar (Hudson, WI)	20079	1:500
Primary	Phospho-ezrin	Rabbit	Cell Signaling (Danvers, MA)	3726S	1:200
Primary	Rotavirus NSP2	Guinea pig	[74][a]		1:500
Secondary	Anti-goat Alexa Fluor 488	Donkey	Life Technologies (Carlsbad, CA)	A11055	1:1000
Secondary	Anti-rabbit Alexa Fluor 488	Donkey	Life Technologies	R37116	1:2000
Secondary	Anti-rabbit Alexa Fluor 555	Donkey	Life Technologies	A31572	1:1000
Secondary	Anti–guinea pig Alexa Fluor 568	Goat	Life Technologies	A11075	1:1000
Secondary	Anti-mouse Alexa Fluor 568	Goat	Life Technologies	A11004	1:2000

NSP, nonstructural protein.
[a]Provided by Mary Estes.

number of ChgA-positive cells ($P < .0001$) (Figure 2*A*, left panel). This pattern also was observed in 2D flat tet*NGN3*-HIEs monolayers, with doxycycline concentrations at or less than 0.01 μg/mL, showing ∼0.4% ChgA-positive cells, similar to the noninduced tet*NGN3*-HIEs (Figure 2*A*, right panel). Treatment of tet*NGN3*-HIEs with 0.1 μg/mL doxycycline resulted in ∼5% ChgA-positive cells, an approximately 12-fold increase, whereas addition of 1 μg/mL doxycycline resulted in ∼40% ChgA-positive cells (Figure 2*A*, right panel). Thus, induction of tet*NGN3* correlated with an increase in ChgA-positive cells, supporting our premise that overexpression of *NGN3* would drive EEC differentiation in HIEs. The tet*NGN3*-HIEs have stably maintained the tet*NGN3* transgene and shown the doxycycline-induced increase in ChgA-positive cells (detected by immunofluorescence staining) for >10 months. In addition, tet*NGN3*-HIEs maintained inducible expression after storage in liquid nitrogen (data not shown).

Induction of Enteroendocrine Cell Differentiation

To confirm that doxycycline treatment alone did not induce EEC differentiation in HIEs, we measured messenger RNA (mRNA) transcript levels after treating the parental (nontransduced) jejunum HIEs with 0 or 1 μg/mL doxycycline. We quantitated the mRNA levels of the enterochromaffin cell markers *CHGA* and *TPH1* and the enterocyte marker villin (*VIL1*) by quantitative polymerase chain reaction (qPCR) (Figure 2*B*, Table 2). No significant difference between treatment groups was present in any of the cell markers examined, indicating that doxycycline alone does not impact EEC differentiation in the absence of *NGN3* expression (Figure 2*B*).

In a complementary approach to show that induction of tet*NGN3* increases EEC differentiation, we correlated the increase in *NGN3* and *CHGA* transcripts in tet*NGN3*-HIEs treated with 0, 0.1, and 1 μg/mL doxycycline, and compared gene expression in the 3 different HIE formats (ie, 3D culture, flat monolayers, and Transwell monolayers), summarized in Table 3. Overall, we observed a doxycycline dose-dependent increase in both *NGN3* and *CHGA* expression in all 3 formats of the tet*NGN3*-HIEs. Treatment with 1 μg/mL doxycycline significantly increased both enterochromaffin cell markers in all 3 culture formats (Figure 2*C*). However, there were some notable differences in the expression profiles between each type of HIE format. Treating 3D tet*NGN3*-HIEs with 0.1 μg/mL doxycycline

Table 2. Primers Used in This Study

Gene	Forward (5') sequence	Reverse (3') sequence	Marker of	Reference
18S	GATATGCTCATGTGGTGTTG	AATCTTCTTCAGTCGCTCCA	Housekeeping	75
LYZ	AAAACCCCAGGAGCAGTTAAT	CAACCCTCTTTGCACAAGCT	Paneth cell	76
LGR5	CTCCCAGGTCTGGTGTGTTG	GAGGTCTAGGTAGGAGGTGAAG	Stem cell	77
MUC2	CTGCACCAAGACCGTCCTCATG	GCAAGGACTGAACAAAGACTCAGA	Goblet cell	78
VIL1	AGCCAGATCACTGCTGAGGT	TGGACAGGTGTTCCTCCTTC	Enterocyte	79
CHGA	TGTAGTGCTGAACCCCCACC	CTCTCGCCTTTCCGGATCT	Enteroendocrine	80
NGN3	*AGTTGGCACTGAGCAAGC*	AGTGCCGAGTTGAGGTTG	Enteroendocrine	71
TPH1	TGGCTGAACCTAGTTTTGCCC	CCAAAGACTCTTAGCTGTCCATC	Enteroendocrine serotonin synthesis	81

Table 3. Fold Changes in *NGN3* and *CHGA* Expression With Doxycycline Treatment

tetNGN3-HIE format	NGN3		CHGA	
	0.1 μg/mL dox	1 μg/mL dox	0.1 μg/mL dox	1 μg/mL dox
3D cultures	1.5	143	14	239
Flat monolayers	12	141	54	316
Transwell monolayers	300	436	326	445

induced *NGN3* and *CHGA* expression to a lesser degree than 0.1 μg/mL doxycycline treatment of flat or Transwell monolayers (Figure 2C), which may be owing to limited penetrance of doxycycline through the Matrigel (Corning Inc, Corning, NY) used for 3D cultures. Furthermore, Transwell monolayers treated with 0.1 μg/mL doxycycline have a greater fold induction of *NGN3* and *CHGA* expression than in flat monolayers (Figure 2C). This difference may be the result of greater cell surface contact with the media in Transwell monolayers, which have both apical and basolateral access to the media, than in flat monolayers. Together, these results show that the inducible tetNGN3-HIEs are a tunable and versatile system for increased differentiation of enterochromaffin cells in each of the HIE culture formats.

Characterization of Epithelial Cell Types Present in tetNGN3-HIEs

To assess the impact of *NGN3* overexpression on HIE morphology, we treated 3D and Transwell monolayer preparations of the tetNGN3-HIEs with 0, 0.1, and 1 μg/mL doxycycline (Figure 3A and B). H&E staining of 3D (Figure 3A) and Transwell monolayers (Figure 3B) showed only minor alterations in morphology upon induction with 0.1 μg/mL doxycycline, primarily larger nuclei and increased cell height (Figure 3B, middle panel). Strong induction with 1 μg/mL doxycycline resulted in more significant morphologic changes. In the 3D tetNGN3-HIEs, there was a marked increase in luminal (apical) cell debris (Figure 3A, right panel), and in Transwell monolayers we observed larger nuclei and a discontinuous apical membrane with increased shedding of cellular material (Figure 3B, right panel). Furthermore, we examined the ultrastructure of the tetNGN3-HIEs using transmission electron microscopy of 3D HIEs treated for 5 days with 0 or 1 μg/mL doxycycline in differentiation media (Figure 3C and D). Most cells observed in the 0 μg/mL doxycycline-treated tetNGN3-HIEs had the basolateral nuclei, apical microvilli, and brush border characteristic of enterocytes (Figure 3C). As expected, in tetNGN3-HIEs treated with 1 μg/mL doxycycline, we observed more EECs based on greater numbers of cells with electron-dense granules, including cells open to the lumen of the 3D enteroid (Figure 3D).

Differentiation of HIEs by exclusion of Wnt3a from the culture media drives maturation of the different epithelial cell types,[14,17,21,44,45] so we next used reverse-transcription qPCR to determine whether *NGN3* induction altered expression of cell lineage–specific marker genes in differentiated HIEs. For this we tested markers for Paneth cells (lysozyme [*LYSZ*]), crypt base columnar stem cells (*LGR5*), goblet cells (mucin 2 [*MUC2*]), and enterocytes *VIL1* and sucrase isomaltase [*SI*]) (Table 2). First, we observed no difference in differentiation marker expression between the parental HIE line and the uninduced tetNGN3-HIEs, indicating that lentivirus transduction itself did not cause alterations in HIE cell differentiation (data not shown). In 3D tetNGN3-HIEs (Figure 4A, left panel), doxycycline induction caused no significant changes in cell lineage–specific gene expression, and although *SI* showed a trend for lower levels, *VIL1* expression remained unchanged. Furthermore, in tetNGN3-HIE flat monolayers the overall gene expression levels were similar to the 3D tetNGN3-HIEs, and no significant changes in lineage-specific marker genes were observed (Figure 4A, right panel).

To gain further insight into the broader impacts of *NGN3* overexpression, we performed global transcriptional analysis of mRNA (RNA sequencing [RNA-seq]) isolated from tetNGN3-HIEs cultured in Transwell format in the absence or presence of 1 μg/mL doxycycline during differentiation for 5 days. Comparison of the expression levels across 31 genes indicated a dramatic increase in the abundance of *NGN3* and *CHGA* transcripts (Figure 4B and Table 4). However, when a 1.5 $\log_2$ cut-off value (corresponding to a 3-fold difference in gene expression) was applied, genes involved in tight junctions, or markers of Paneth, goblet, or tuft cell lineages, were not altered significantly. In contrast, all markers of enterocytes decreased modestly, with $\log_2$ fold changes of ~ 2 (Figure 4B and Table 4). Similar to the H&E staining (Figure 3), immunofluorescence microscopy of 3D cultures and Transwell monolayers showed that the tetNGN3-HIEs maintained a polarized cell layer upon doxycycline treatment, as shown by apical localization of phospho-ezrin, SI, and sodium-glucose transporter 1 (Figure 4C–E). Finally, we examined whether *NGN3* overexpression altered goblet cell numbers in the tetNGN3-HIEs. Immunostaining for Muc2 in noninduced or induced (1 μg/mL doxycycline) 3D tetNGN3-HIEs showed that induction of *NGN3* expression did not decrease the number of Muc2-positive cells (Figure 4F), which is consistent with the lack of changes in *MUC2* gene expression between 0 and 1 μg/mL doxycycline treatments found by qPCR and RNA-seq analyses (Figure 4A and B). Taken together, inducible *NGN3* overexpression significantly increased the EEC population, but this did not substantially change the transcript levels of other differentiated cell types or the morphologic characteristics of these enteroids.

tetNGN3-HIEs Secrete Serotonin in Response to Physiological Stimuli

The enterochromaffin cell subtype is an important source of serotonin-mediated signaling, which has multiple effects on intestinal homeostasis, and disruptions in serotonin signaling have been shown to contribute to several GI disorders.[46–52] Serotonin is synthesized via the conversion of L-tryptophan by the enzyme tryptophan hydroxylase, and
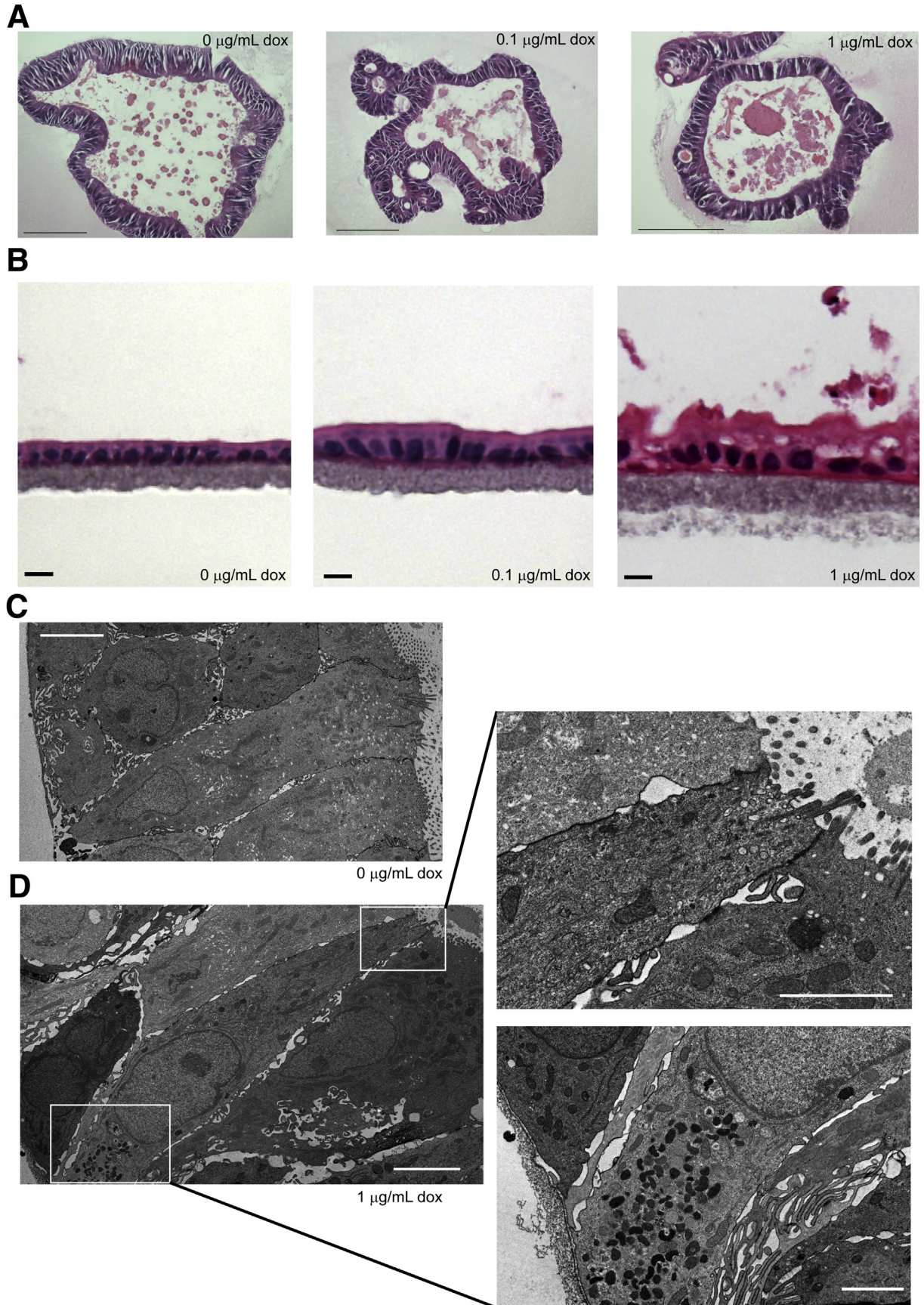
stored in secretory vesicles for stimulus-driven secretion.[53] Therefore, we tested if induction of NGN3 overexpression in HIEs increased serotonin response to biological stimuli in vitro. We confirmed that both CHGA and TPH1 gene expression are up-regulated in doxycycline-induced tetNGN3-HIEs (Figure 5A). Furthermore, we showed that doxycycline induction (1 μg/mL) increased the number of ChgA and serotonin double-positive cells by fluorescence of 3D tetNGN3-HIEs (Figure 5B). These indicate an increase in the number of serotonin-secreting enterochromaffin cells.

We next characterized the physiological response of the tetNGN3-HIE–derived enterochromaffin cells to stimuli previously shown to elicit serotonin secretion by other enterochromaffin model systems.[54,55] A previous study found that mouse enterochromaffin cells secrete serotonin in response to norepinephrine and isovalerate.[54] Norepinephrine is a neurotransmitter important for communication between the gut and the enteric nervous system, particularly in response to infection or injury.[56] Isovalerate is a fatty acid metabolite likely generated by the microbiome, particularly by amino acid fermenting bacteria such as from the Clostridial, Bacillus, Lactobacillus, Streptococcus, and Proteobacteria groups.[57] We quantified serotonin secretion into the media of flat monolayers of tetNGN3-HIEs, induced with 0 or 1 μg/mL doxycycline, and treated with different concentrations of norepinephrine or isovalerate. After stimulation with these agonists, supernatants were collected to measure serotonin secretion using a serotonin enzyme-linked immunosorbent assay. We found that norepinephrine treatment of induced tetNGN3-HIEs stimulated a significant and dose-dependent increase in serotonin secretion, but no increase in serotonin secretion was observed from the noninduced tetNGN3-HIEs ($P < .05$, $P < .0001$) (Figure 5C). Interestingly, treatment with up to 500 μmol/L isovalerate did not stimulate measurable serotonin secretion in either the noninduced or the doxycycline-induced tetNGN3-HIEs (Figure 5D).

To determine if our model was responsive to other microbial stimuli, we tested whether rotavirus (RV) infection, a common diarrhea-causing enteric virus, stimulates serotonin secretion from tetNGN3-HIEs. Previous studies in both human enterochromaffin cell lines, and in mice, found that RV infects both enterocytes and ChgA- and serotonin-positive enterochromaffin cells and stimulates serotonin secretion.[12,55] Furthermore, HIEs are a new model for RV infection and enterochromaffin cells in HIEs support RV infection; however, whether RV infection stimulates serotonin secretion in HIEs has not been tested.[13,14] Flat monolayers of tetNGN3-HIE induced with 0 or 1 μg/mL doxycycline were infected with trypsin-activated human RV

(strain Ito, G3[P8]). Supernatants were harvested at 24 hours after infection to measure serotonin secretion. RV infection significantly increased serotonin secretion in both the noninduced and doxycycline-induced tetNGN3-HIEs compared with mock-infected tetNGN3-HIEs ($P < .0001$) (Figure 5E). Most notably, the serotonin response to RV infection was significantly greater from the doxycycline-induced tetNGN3-HIEs, showing that the tetNGN3-HIEs amplify observed enterochromaffin cell responses (Figure 5E).

The ability of RV to stimulate serotonin secretion in tetNGN3-HIEs also was tested in Transwell monolayers that were induced with 0.1 μg/mL doxycycline in differentiation media for 5 days. In Transwell monolayers we were able to test serotonin secretion both apically and basolaterally after infection with RV at 1 hours postinfection (hpi), 12 hpi, and 24 hpi (Figure 5F and G). At 12 hpi, RV-infected Transwell monolayers secreted significantly more serotonin into the basolateral compartment than mock-infected monolayers ($P < .05$) (Figure 5G), while apical serotonin secretion was not increased significantly (Figure 5F). By 24 hpi, there was significantly more serotonin secretion both apically and basolaterally from RV-infected than mock-infected monolayers ($P < .01$) (Figure 5G and F). These data indicate that serotonin primarily is secreted basolaterally from the monolayer, particularly early in RV infection, but both basolateral and apical serotonin secretion is detected later in infection. Finally, we confirmed that the doxycycline-induced enterochromaffin cells are susceptible to RV infection by immunofluorescence confocal microscopy. At 12 hpi, the tetNGN3-HIE Transwell monolayers were fix and stained for ChgA and the RV nonstructural protein 2, which shows co-immunostaining of cells for ChgA and nonstructural protein 2 (Figure 5H) that is consistent with the known susceptibility of enterochromaffin cells to RV infection.[12,13,55]

tetNGN3-HIEs Differentiate Into Multiple Enteroendocrine Cell Types

To identify other EEC types that are present in the induced tetNGN3-HIEs, we examined the RNA-seq data from doxycycline-induced tetNGN3-HIEs for expression of marker genes predominantly expressed in the 7 EEC subtypes, as well as marker genes for enterochromaffin cells. We found that expression of each of the EEC marker genes was up-regulated to varying degrees (Figure 6A and Table 4), suggesting that doxycycline treatment of the tetNGN3-HIEs could induce the other EEC cell types in addition to enterochromaffin cells. These results are supported by

---

Figure 3. (*See previous page*). **tetNGN3-HIEs maintain cellular morphology in culture.** H&E-stained (*A*) 3D (*scale bar*: 100 μm) and (*B*) Transwell monolayer (*scale bar*: 10 μm) tetNGN3-HIEs treated with 0, 0.1, or 1 μg/mL doxycycline. Images were acquired using a 20× Plan Apo (NA, 0.75) DIC objective on an upright Nikon Eclipse 90i microscope with a DS-Fi1-U2 camera and Nikon Elements software. Transmission electron micrographs H&E of 3-D tetNGN3-HIEs with (*C*) 0 μg/mL (*scale bar*: 4 μm; original magnification, 1500×) or (*D*) 1 μg/mL doxycycline (*left scale bars*: 4 μm; original magnification, 1500×; *right scale bars*: 2 μm; original magnification, 3000×). Transmission electron micrograph sections were viewed on a Hitachi H7500 transmission electron microscope set to 80 kV and collected using an AMT XR-16 digital camera and AMT Image Capture, v602.600.51 software.
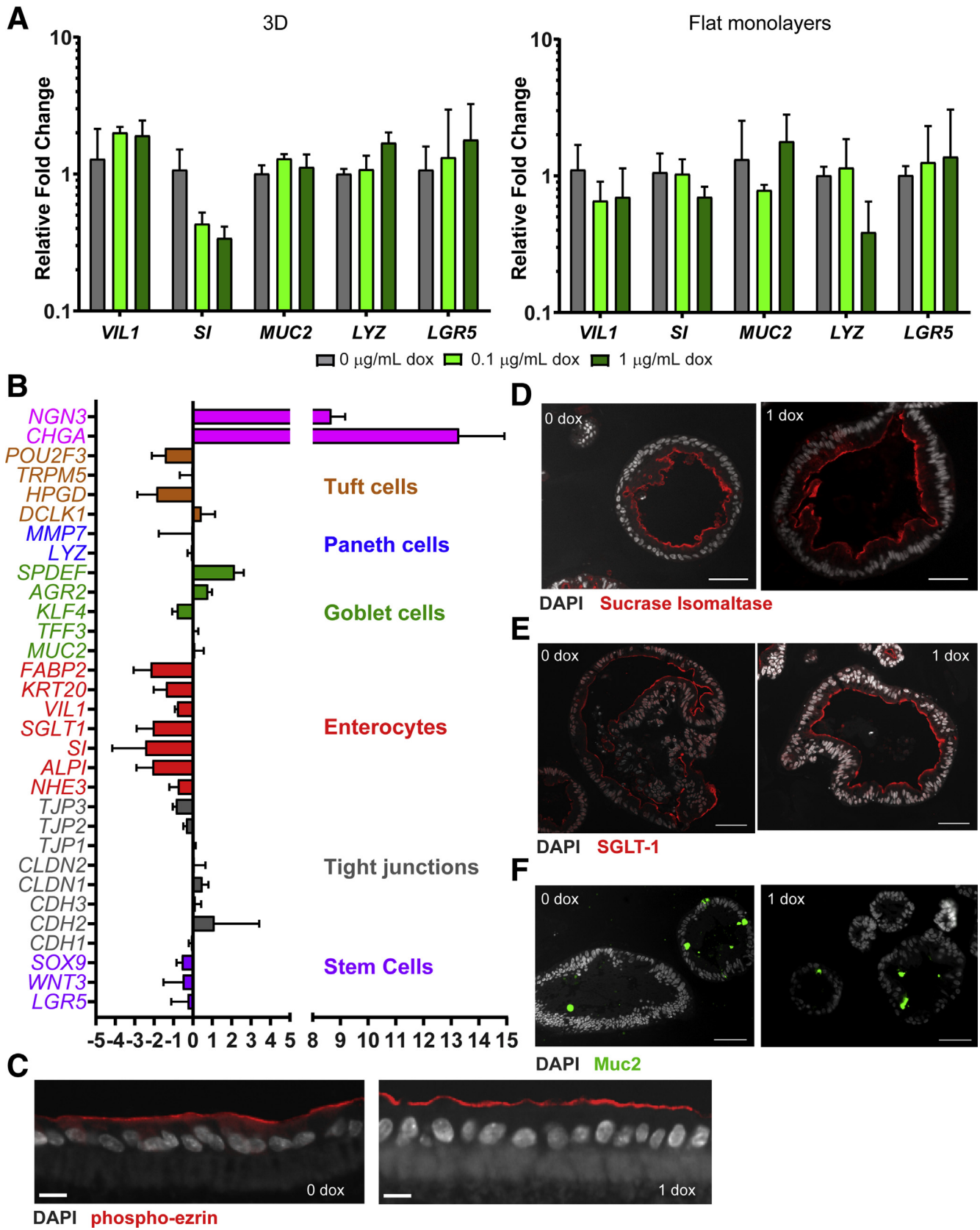
positive immunostaining for GLP-1 distinct from ChgA-positive cells in tet*NGN3*-HIE monolayers when induced with 1 μg/mL doxycycline (Figure 6*B*). To test if doxycycline-induced tet*NGN3*-HIEs functionally amplified the physiological response of these EEC subtypes, we quantified gut hormones known to be secreted by different EEC types after stimulation with norepinephrine or infection with RV, as in the experiments described earlier (Figure 6*C–F*). We did not detect secreted hormones from uninduced tet*NGN3*-HIE monolayers after stimulation with norepinephrine or RV infection, with the exception of MCP-1, which also is known to be produced by enterocytes (Figure 6*C* and *D*). In contrast, tet*NGN3*-HIE monolayers induced with 1 μg/mL doxycycline showed increased secretion of MCP-1 and GIP (from K cells) in response to 5 μmol/L norepinephrine (Figure 6*B*). Of note, norepinephrine did not stimulate PYY (L cells) or ghrelin (P/D1 cells). Furthermore, in response to RV infection, the induced tet*NGN3*-HIEs secreted large quantities of MCP-1 and GIP and moderate amounts of PYY and ghrelin (Figure 6*E*), and this response was absent in uninduced tet*NGN3* HIEs (Figure 6*D*). Norepinephrine and RV infection did not stimulate pancreatic polypeptide (PP) cell (also known as F cells) secretion, which is produced primarily in pancreatic cells and only rarely in the intestine.[58] Several other hormones in the multiplexed metabolic assay were lower than the levels of detection including tumor necrosis factor-α (TNF-α), amylin, C peptide, glucagon, interleukin (IL)6, and leptin. Together, these data show that our tet*NGN3*-HIE model drives the differentiation of multiple functional EEC subtypes that secrete gut hormones in response to biologically relevant stimuli.

Discussion

Limitations of the available human EEC systems have made it challenging to comprehensively study the molecular physiology of EECs. In this study, we engineered a HIE line to have inducible overexpression of *NGN3* that enables vast up-regulation of EEC numbers in the HIEs. For the characterization of the tet*NGN3*-HIEs, we initially focused on enterochromaffin cells because they are the dominant intestinal EEC subtype and of great interest for EEC biology and serve a key role in sensing/responding to microbial metabolites and intestinal pathophysiology.[59–61] We showed that doxycycline-induced *NGN3* overexpression in human jejunal intestinal enteroids increased EECs, as measured by mRNA and protein expression of the endocrine marker *CHGA*. This response was doxycycline–dose-

dependent, showing that the tet*NGN3*-HIEs allow for tunable customization of the number of EECs in different HIE formats (eg, 3D, flat monolayers, and Transwell monolayers). Global analysis of transcriptional changes with *NGN3* induction indicated no significant differences in markers of stem cells, tight junctions, tuft cells, Paneth cells, or goblet cells, and a slight decrease in enterocyte markers compared with noninduced HIEs. Furthermore, in response to known stimuli, differentiated tet*NGN3*-HIEs release serotonin and several gut hormones characteristic of K cell, L cell, and enterochromaffin cell populations in a single culture system.[12,54,55]

The tet*NGN3*-HIE model system described in this work overcomes some of the limitations associated with the existing models of EECs. In contrast to primary EECs isolated from tissue and cancer-derived cell lines, HIOs and HIEs are more robust and renewable model systems for studying EECs.[29,54,62,63] However, similar to the intestine, few EECs spontaneously develop in both HIOs and HIEs, so the rarity of EEC cells remains a limitation of native organoid/enteroid cultures. Thus, increasing *NGN3* expression to drive EEC differentiation, as has been done in recent work with HIOs, is an effective strategy to increase the abundance of EECs for study.[29,40,64] In HIOs, *NGN3* overexpression increased the number of ChgA-positive cells to 5% using adenovirus-based constitutive expression and to 23% using lentivirus-based, doxycycline-inducible expression.[29,40,64] This is comparable with our results with the tet*NGN3*-HIEs wherein we obtained 40% ChgA-positive cells using a lentivirus-based inducible *NGN3* overexpression strategy. These results indicate that for both HIOs and HIEs, stably engineering the stem cell to have inducible expression of *NGN3* is an efficient approach to drive differentiation of higher numbers of EECs.

Together, the use of inducible *NGN3* expression in HIOs and HIEs establish complementary systems that will be widely useful to investigate different aspects of EEC interactions in the GI tract. In the tet*NGN3*-HIE model, the HIEs are derived from undifferentiated adult stem cells, and therefore will be particularly useful for studies of adult intestinal epithelial cell expression, function, and physiology. Indeed, isolation, establishment, and transduction of enteroids from individual patients to assess EEC function or response to drug treatments may be a future strategy for personalized medicine.[65] Although HIOs are composed of both epithelial and mesenchymal cells, HIEs consist of only epithelial cells so the tet*NGN3*-HIEs allow direct study of EEC interactions with other intestinal epithelial cells. In addition, co-culture studies that combine the tet*NGN3*-HIEs

Figure 4. (*See previous page*). **Characterization of epithelial cell types in doxycycline-induced tet*NGN3*-HIEs.** (*A*) qPCR of cell marker mRNA transcripts normalized to 18S mRNA transcripts in tet*NGN3*-HIE 3D cultures and flat monolayers (n = 3 biological replicates). (*B*) Log$_2$ fold expression of fragments per kilobase of transcript per million mapped reads (FPKM) values from RNA-seq analysis comparing gene expression in 1 μg/mL doxycycline with gene expression in 0 μg/mL doxycycline (n = 6 biological replicates). (*C*) Transwell monolayers and (*D–F*) 3D cultures were treated with 0 or 1 μg/mL doxycycline and fixed and stained. Immunofluorescence staining for (*C*) phospho-ezrin (Alexa Fluor 555, red), (*D*) sucrase isomaltase (Alexa Fluor 555, red), and (*E*) sodium-glucose transporter 1 (Alexa Fluor 555, red) to mark the apical border and (*F*) for muc2 (Alexa Fluor 488, green) to mark goblet cells and counterstained with DAPI (blue). Images were acquired using a 20× Plan Apo (NA, 0.75) DIC objective on an upright Nikon Eclipse 90i microscope with a Photometrics CoolSNAP HQ2 camera and Nikon Elements software. *Scale bars*: (*C*) 10 μm, (*D–F*) 50 μm.

Table 4. RNA-Seq Analysis of Gene Expression With and Without Doxycycline Treatment

Gene symbol	Gene	Marker of	Average FPKM 0 dox (n = 6)	Average FPKM 1 dox (n = 6)	Fold change FPKM	SD	Log$_2$ fold change FPKM	SD
LGR5	Leucine-rich repeat containing G-protein–coupled receptor 5	Stem cells	0.04	0.03	0.94	0.50	-0.28	0.842
WNT3a	Wnt family member 3A	Stem cells	0.03	0.01	0.81	0.39	-0.53	0.993
SOX9	SRY-box 9	Stem cells	14.53	9.07	0.68	0.12	-0.58	0.267
CDH1	Cadherin 1	Tight junctions	160.23	150.63	0.93	0.08	-0.10	0.122
CDH2	Cadherin 2	Tight junctions	0.16	0.21	4.80	4.09	1.12	2.303
CDH3	Cadherin 3	Tight junctions	13.50	15.31	1.12	0.23	0.14	0.285
CLDN1	Claudin 1	Tight junctions	25.07	35.81	1.43	0.29	0.49	0.302
CLDN2	Claudin 2	Tight junctions	5.89	6.42	1.14	0.47	0.09	0.552
TJP1	Tight junction protein 1	Tight junctions	10.36	10.56	1.03	0.08	0.03	0.114
TJP2	Tight junction protein 2	Tight junctions	52.97	41.06	0.79	0.08	-0.35	0.143
TJP3	Tight junction protein 3	Tight junctions	130.96	71.40	0.55	0.07	-0.88	0.159
NHE3	Solute carrier family 9 member A3	Enterocytes	88.57	51.75	0.61	0.19	-0.78	0.443
ALPI	Alkaline phosphatase	Enterocytes	36.40	11.07	0.27	0.13	-2.09	0.818
SI	Sucrose isomaltase	Enterocytes	71.42	18.61	0.29	0.25	-2.46	1.697
SGLT	Solute carrier family 5 member 1	Enterocytes	149.85	40.17	0.27	0.14	-2.07	0.837
VIL1	Villin	Enterocytes	307.23	173.99	0.57	0.04	-0.82	0.106
KRT20	Keratin 20	Enterocytes	1582.92	633.48	0.41	0.17	-1.39	0.635
FABP2	Fatty acid binding protein 2	Enterocytes	135.33	37.90	0.25	0.14	-2.18	0.882
MUC2	Mucin 2	Goblet cells	3.29	3.50	1.13	0.35	0.12	0.445
TFF3	Trefoil factor 3	Goblet cells	3161.12	3255.62	1.04	0.17	0.04	0.239
KLF4	Kruppel-like factor 4	Goblet cells	51.85	28.74	0.57	0.09	-0.83	0.238
AGR2	Anterior gradient 2	Goblet cells	217.95	380.20	1.74	0.24	0.79	0.196
SPDEF	SAM pointed domain containing ETS transcription factor	Goblet cells	1.44	6.74	4.66	1.38	2.16	0.462
LYZ	Lysozyme	Paneth cells	367.25	346.23	0.94	0.12	-0.10	0.178
MMP7	Matrix metallopeptidase 7	Paneth cells	10.30	10.97	1.53	1.46	-0.08	1.676
DCLK1	Double cortin-like kinase 1	Tuft cells	0.01	0.01	1.52	0.82	0.45	0.687
HPGD	15-hydroxyprostaglandin dehydrogenase	Tuft cells	130.38	38.04	0.33	0.21	-1.88	0.981
TRPM5	Transient receptor potential cation channel subfamily M member 5	Tuft cells	0.99	0.91	1.01	0.40	-0.08	0.593
POU2F3	POU class 2 homeobox 3	Tuft cells	0.59	0.24	0.40	0.19	-1.45	0.675
NGN3	Neurogenin-3	Enteroendocrine	1.75	678.66	428.67	141.38	8.68	0.494
CHGA	Chromogranin A	Enteroendocrine	1.91	11,127.90	17,779.46	23,032.47	13.29	1.63
TPH1	Tryptophan hydroxylase 1	Enteroendocrine	0.03	50.41	3054.77	251.17	11.17	1.25
PAX6	Paired box 6	Enteroendocrine	0.09	5.53	75.60	43.61	5.97	0.96
NEUROD1	Neuronal differentiation 1	Enteroendocrine	0.03	85.65	5073.90	2738.32	11.83	1.39
GIP	Gastric inhibitory polypeptide	Enteroendocrine, subtype K	0.16	91.53	6926.92	3346.00	11.26	2.63
GHRL	Ghrelin prepropeptide	Enteroendocrine, subtype K	0.28	327.97	1576.15	1351.91	10.33	0.90
SST	Somatostatin	Enteroendocrine, subtype D	0.76	448.36	6733.26	3495.26	10.93	2.62
PAX4	Paired box 4	Enteroendocrine, subtype D	0.04	64.10	3468.87	1504.07	11.32	1.22

Table 4. Continued

Gene symbol	Gene	Marker of	Average FPKM 0 dox (n = 6)	Average FPKM 1 dox (n = 6)	Fold change FPKM	SD	Log$_2$ fold change FPKM	SD
GLP1	Glucagon-like peptide 1	Enteroendocrine, subtype L	0.04	0.37	15.62	11.63	3.54	1.13
PYY	Peptide YY	Enteroendocrine, subtype L	0.15	0.41	5.65	2.68	1.73	0.646
GAST	Gastrin	Enteroendocrine, subtype G	0.32	2.46	46.49	35.50	4.53	2.04
SCT	Secretin	Enteroendocrine, subtype S	1.02	3.68	7.37	3.617	2.301	1.47
CCK	Cholecystokinin	Enteroendocrine, subtype I	0.03	0.67	39.66	26.75	4.57	1.88
MLN	Motilin	Enteroendocrine, subtype M	1.62	3404.32	14,6280.01	22,926.82	13.55	4.13

dox, doxycycline; FPKM, fragments per kilobase per million mapped reads POU, Pituitary-specific Octamer transcription factor Unc-86; SAM, S-adenosylmethionine uptake transporter.

with other cell types, such as immune cells, endothelial cells, and neurons, will be facilitated by the adaptability of HIEs to different culture formats (3D, 2D, and Transwells), which is unique to HIE cultures. Finally, induction and differentiation of tetNGN3-HIEs yields EECs in 6–7 days, which may be a simpler and faster system for generating increased numbers of EECs for higher-throughput studies of EEC responses to microbial, diet, or environmental stimuli.

The induced EECs from tetNGN3-HIEs show strong functional responses to both norepinephrine and RV infection. Both norepinephrine and RV infection increased secretion of serotonin, MCP-1, and GIP, but RV infection also elicited secretion of PYY and ghrelin. Thus, this system shows distinct functional responses to different stimuli. HIEs have been established as a new, biologically relevant system to study RV-induced gut hormone secretion. RV infects enterochromaffin cells in HIEs and induces serotonin secretion both in mice and in vitro from GOT1 cells.[12–14] Here, we show that RV infection of tetNGN3-HIEs induced serotonin secretion, but this response was amplified significantly by doxycycline induction to increase EECs. By using Transwell monolayers, we were able to show that serotonin is secreted both apically and basolaterally, although it is possible that some basolateral-to-apical diffusion of serotonin occurs, potentially through damaged tight junctions.[12,55] RV also induced secretion of GIP, PYY, and ghrelin, which was detected only from doxycycline-induced tetNGN3-HIEs and indicates that biological responses from rare EECs may be missed in native enteroids. These finding highlights the potential tetNGN3-HIEs have for molecular discovery, because secretion of GIP, PYY, and ghrelin during RV infection to the best of our knowledge has not been identified previously, so whether RV infects these EEC subtypes or secretion of these hormones occurs through other signaling pathways merits future investigation.[66] Finally, because insults to the epithelium increase levels of catecholamines (eg, norepinephrine), the sensitivity of tetNGN3-HIEs to norepinephrine makes them a good model for co-culture studies to measure EEC responses to inflammation or infection.[50,52]

The tetNGN3-HIEs are a robust and versatile system for induction of EECs, but some limitations and unknowns about this new model remain. First, the induction of EECs in this system requires lentivirus integration of a recombinant NGN3 gene, making these an engineered intestinal organoid system. An alternative approach to induce endogenous EECs in mouse intestinal organoids was established through the combined inhibition of WNT, Notch, and epidermal growth factor receptor (ie, mitogen-activated protein kinase) signaling pathways.[67] This method leads to increased EEC differentiation, with a concomitant decrease in Paneth and goblet cell numbers.[67] In contrast, the tetNGN3-HIEs maintained markers of both Paneth and goblet cells, suggesting that NGN3 expression alone is insufficient to abolish these other lineage pathways. Second, using this HIE model, we observed increases in most EEC subtypes by RNA-seq and measured hormone secretion from enterochromaffin, L, K, and P/D1 cell subtypes. Although beyond the scope of this study, further studies are needed to determine whether the other subtypes also are functionally responsive to stimuli.[68–73] Third, we observed no differences in stem cell gene expression in differentiated enteroids with or without NGN3 induction. However, we did not examine the overall effects of NGN3 overexpression on the stem cell niche in this HIE model. Further studies may elucidate if increased EECs and hormone secretion modulate the stem cell response to injury or infection. Finally, the tetNGN3-HIEs did not secrete serotonin in response to the short-chain fatty acid isovalerate, in contrast to recent studies using enteroids derived from ChgA-enhanced Green Fluorescent Protein (EGFP) reporter mice (segment not specified).[54] Inherent differences between the 2 systems, such as different receptor expression between human beings and mice or between intestinal segments, may account for the different responses.

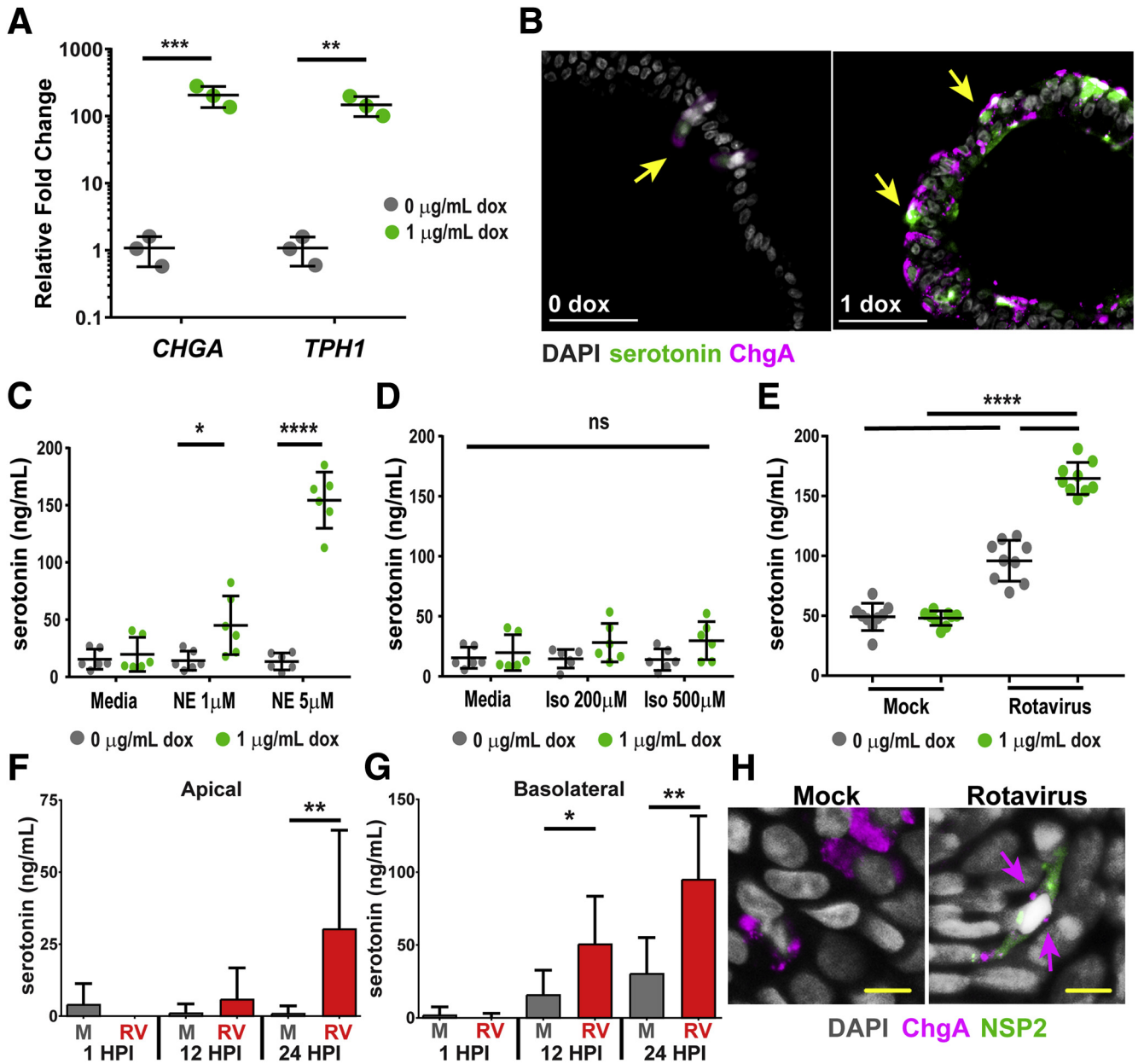The tetNGN3-HIE system is a new and powerful tool for investigating the roles of EECs in microbial-environment-host

Figure 5. tet*NGN3*-HIEs produce serotonin in response to physiological stimuli. (*A*) qPCR of *CHGA* and tryptophan hydroxylase-1 (*TPH1*) mRNA transcripts normalized to 18S mRNA transcripts. n = 3 biological replicates. (*B*) 3D tetNGN3-HIEs were treated with 0 or 1 μg/mL doxycycline (dox) and fixed and immunostained for ChgA (Alexa Fluor 555, pink) and serotonin (Alexa Fluor 488, green), and counterstained with DAPI (gray). Some cells were double-positive for ChgA and serotonin (*yellow arrows*). Images were acquired using a 20× Plan Apo (NA, 0.75) DIC objective on an upright Nikon Eclipse 90i microscope with a Photometrics CoolSNAP HQ2 camera and Nikon Elements software. *Scale bar*: 50 μm. (*C–E*) tet*NGN3*-HIE flat monolayers were induced with 0 or 1 μg/mL doxycycline. Serotonin release as measured by enzyme-linked immunosorbent assay: (*C*) after 2-hour treatment with norepinephrine (NE) (n = 2 biological replicates), (*D*) after 2-hour treatment with isovalerate (Iso) (n = 2 biological replicates), and (*E*) after 24 hpi with rotavirus (n = 3 biological replicates). (*F* and *G*) tet*NGN3*-HIE Transwell monolayers were differentiated for 5 days with 0.1 μg/mL doxycycline and mock or RV-infected. Serotonin release measured by enzyme-linked immunosorbent assay from (*F*) apical or (*G*) basal Transwell compartments. (*H*) Maximum intensity projection images of confocal Z-stack of Transwell monolayers fixed and stained for rotavirus nonstructural protein 2 (NSP2) (Alexa Fluor 488, green) and ChgA (Alexa Fluor 568, pink, *arrows*), and counterstained with DAPI (gray) using a Plan Apo VC 60× Oil DIC objective on a Nikon A1plus point scanning confocal microscope. *Scale bar*: 10 μm. *$P < .05$, **$P < .01$, ***$P < .001$, and ****$P < .0001$.
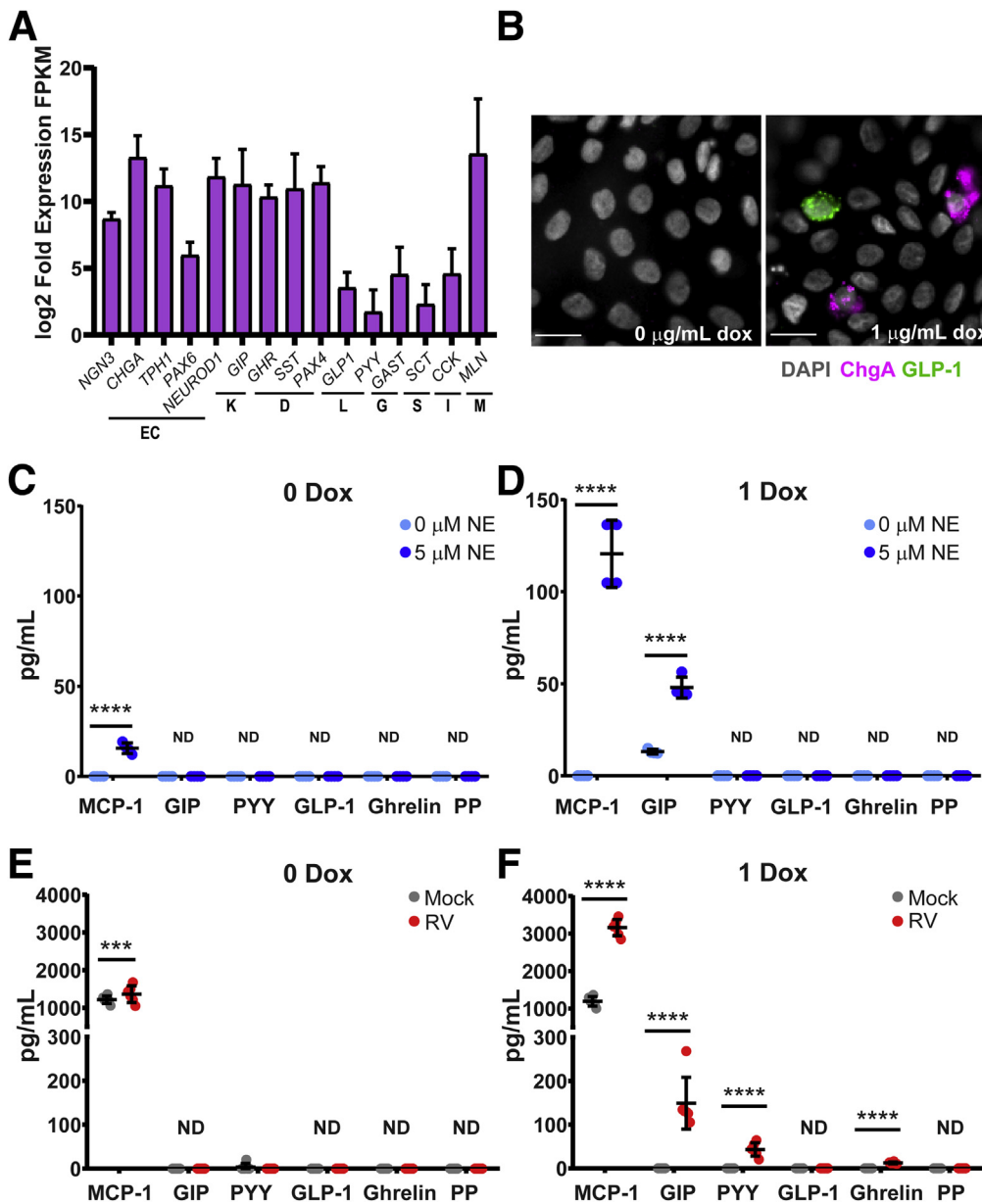
Figure 6. tetNGN3-HIEs differentiate into other EEC types. (A) Log$_2$ fold expression of fragments per kilobase of transcript per million mapped reads (FPKM) values from RNA-seq comparing gene expression in 1 μg/mL doxycycline with gene expression in 0 μg/mL doxycycline. n = 6 biological replicates. (B) Images of monolayers fixed and stained for ChgA (Alexa Fluor 488, pink) and GLP-1 (Alexa Fluor 568, green) counterstained with DAPI (gray). Images were acquired using a 40× Apo (NA, 1.15) DIC water objective on an inverted Nikon TiE microscope with an ORCA-Flash 4.0 sCMOS camera and Nikon Elements software. Supernatants from tetNGN3-HIEs were induced with (C and E) 0 μg/mL doxycycline (dox) or (D and F) 1 μg/mL dox and collected after (C and D) a 2-hour stimulation with norepinephrine (NE) (n = 2 biological replicates) or (E and F) 24 hpi with RV (n = 3 biological replicates) and secreted products quantitated by Luminex (MCP-1, GIP, PYY, GLP-1, and PP). Scale bar: 20 μm. ***P < .001 and ****P < .0001.

communication, infection, inflammation, and metabolism. Doxycycline induction of the tetNGN3-HIEs generates large numbers of EECs and amplifies EEC responses to biologically relevant stimuli, yet these cultures retain the salient characteristics of HIEs. Furthermore, this is an adaptable system in terms of both regulating the number of EECs and culture formats, which enables greater throughput and functional characterization of EEC responses to a multitude of stimuli. The ability of tetNGN3-HIEs to differentially respond to norepinephrine and RV infection suggests this new model system is well-suited to study the EEC modulatory effects of commensal microbes, microbial metabolites, pathogens, and inflammatory mediators involved in epithelial health and disease.

Materials and Methods
Establishment of HIE Cultures

HIE cultures were generated from crypts isolated from the jejunal tissues of adult patients undergoing bariatric surgery as previously described.[13] These established cultures were obtained at Baylor College of Medicine through the Texas Medical Center Digestive Diseases Center Gastrointestinal Experimental Model Systems (GEMS) Core. Three-dimensional HIE cultures were prepared from the tissue samples and maintained in culture as described previously.[13,17] For these studies, jejunum HIEs from patient J2 were used. Complete medium without growth factors (CMGF-) and CMGF+ were prepared as previously described.[13,17] Briefly, CMGF- consisted of advanced

Dulbecco's modified Eagle medium (DMEM)/F-12 medium supplemented with 100 U/mL penicillin-streptomycin, 10 mmol/L HEPES buffer, and 1× GlutaMAX (all Invitrogen, Carlsbad, CA). CMGF+ consisted of CMGF- medium with 50% (vol/vol) Wnt3A-conditioned medium, 20% (vol/vol) R-spondin–conditioned medium, 10% (vol/vol) Noggin-conditioned medium, 1× B-27 supplement (Invitrogen), 1× N-2 supplement (Invitrogen), 1 mmol/L N-acetylcysteine (Sigma-Aldrich, St. Louis, MO), 50 ng/mL mouse epidermal growth factor (Invitrogen), 10 mmol/L nicotinamide (Sigma-Aldrich), 10 nmol/L Leu-Gastrin I (Sigma-Aldrich), 500 nmol/L A-83-01 (Tocris Bioscience, Bristol, UK), and 10 nmol/L SB202190 (Sigma-Aldrich).

Differentiation medium consisted of the same components as CMGF+ without Wnt3A-conditioned medium, R-spondin–conditioned medium, SB202190, and nicotinamide, and only 5% (vol/vol) Noggin-conditioned medium. hW-CMGF+, for creating and maintaining lentivirus-transduced HIEs, consisted of CMGF+ mixed with an additional 50% (vol/vol) Wnt3a-conditioned medium. All HIEs were passaged in phenol red-free, growth factor–reduced Matrigel (Corning, Corning, NY).

Creation of NGN3-Expressing HIEs

Tetracycline-inducible tet*NGN3*-expressing HIEs were created using lentivirus transduction. The tet*NGN3* lentivirus transfer plasmid was in the pINDUCER backbone and was a kind gift from Dr Noah Shroyer and Dr Jim Wells.[41,64] The tet*NGN3* lentiviruses were packaged and harvested in-house with the packaging plasmid psPAX2, a gift from Dr Didier Trono (Addgene plasmid 12260, Watertown, MA), and the envelope plasmid pCMV-VSV-G, a gift from Dr Bob Weinberg (Addgene plasmid 8454), as described in more detail previously.[42] Virus packaging was assessed using Lenti-X GoStix (Clontech, Mountain View, CA) but virus titers were not otherwise measured. Densely seeded jejunum HIEs were grown in hW-CMGF+ for 1 week to increase stem cell counts. HIEs were dissociated from Matrigel (Corning) with ice-cold 1× phosphate-buffered saline (PBS) and pipetted into 1.7-mL centrifugation tubes for centrifugation in a swinging bucket rotor at 200 × *g* for 5 minutes at 4°C. Supernatant was removed, HIEs were resuspended and washed twice with 1 mL ice-cold 1× PBS, and centrifuged using the same conditions. Supernatants were removed and HIEs were resuspended with lentivirus inoculum consisting of 8 μg/mL polybrene (EMD Millipore, Burlington, MA), 10 μmol/L Y-27632 Rock inhibitor (Tocris Bioscience Bristol, UK), 50 μL tet*NGN3* lentivirus, and freshly made hW-CMGF+ for a total volume of 200 μL. HIEs were incubated with the inoculum in closed centrifugation tubes for 24 hours at 37°C in a humidified 5% CO_2 incubator. After 24 hours, HIEs were centrifuged again and washed twice with ice-cold 1× PBS followed by suspension in Matrigel drops on a 24-well plate. After Matrigel polymerization in the incubator for 10 minutes, 500 μL of hW-CMGF+ medium was added to the well. Media was changed every other day for 1 week before passaging and selecting with 200 μg/mL Geneticin (VWR Radnor, PA). We refer to

this transduced line as tet*NGN3*-HIEs, and they were grown in hW-CMGF+ with 200 μg/mL Geneticin.

Preparation and Differentiation of HIE Monolayers

HIE monolayers were prepared from 3D cultures and seeded into flat 96-well plates or Transwells as described previously.[21,44] In brief, 96-wells or Transwell inserts (Corning, catalog no 3413) were pretreated with Matrigel diluted in 1× PBS (1:40) and incubated at 37°C. 3D HIEs were lifted from Matrigel and washed with an ice-cold solution of 0.5 mmol/L EDTA in 1× PBS and dissociated with 0.05% trypsin/ 0.5 mmol/L EDTA for 4 minutes at 37°C. Trypsin was inactivated with CMGF- + 10% fetal bovine serum and the cell solution was pipetted vigorously and filtered using a 40-μm nylon cell strainer (Corning, catalog no 352340) to dissociate into single cells. Then cells were centrifuged for 5 minutes at 400 × *g*, resuspended with CMGF+ and 10 μmol/L Y-27632 Rock inhibitor, and plated into prepared wells. After 48 hours in CMGF+ and 10 μmol/L Y-27632 Rock inhibitor, the medium was changed to differentiation media with the addition of 10 μmol/L Y-27632 Rock inhibitor and indicated concentrations of doxycycline (Thermo Fisher Scientific, Waltham, MA). Differentiation medium with Y-27632 and doxycycline was changed every day for 4–5 days to differentiate cells.

Immunofluorescence of HIE Monolayers

HIE flat monolayers (2D) were fixed using the BD Cytofix/Cytoperm kit (catalog no 554714; BD Biosciences, San Jose, CA) according to the manufacturer's instructions. Primary antibodies were diluted in BD Perm/Wash buffer (Table 1) and were incubated at 4°C overnight. Primary antibodies were recognized by the appropriate secondary antibodies (Table 1) and incubated for 1 hour at room temperature. Nuclei were stained with 4',6-diamidino-2-phenylindole (DAPI) (catalog no R37606; Thermo Fisher Scientific, Waltham, MA) for 5 minutes at room temperature and washed with 1× PBS for imaging and storage.

Immunofluorescence of Paraffin-Embedded Sections

HIEs (3D) embedded in Matrigel were gently removed and transferred to 1-mL syringes. The cells then were fixed in 4% (vol/vol) paraformaldehyde solution for 1 hour at room temperature. After fixation, cells were deposited into a cassette for paraffin embedding. For Transwell cross-sections, HIE membranes were cut from Transwells, fixed in 4% (vol/vol) paraformaldehyde solution for 1 hour at room temperature, and placed into cassettes for paraffin embedding. Paraffin-embedded sections of 7 μm in thickness were subjected to a series of dehydration steps. Epitope retrieval was performed by incubating slides with Vector Labs Antigen Unmasking Solution Citrate Buffer pH 6 (catalog no H-3300, Burlingame, CA) for 20 minutes at 100°C in a steamer. Slides then were blocked for 1 hour at room temperature in 10% goat and/or donkey serum. Primary antibodies (Table 1) were incubated at 4°C overnight. Primary antibodies were recognized by the appropriate secondary antibodies (Table 1) and incubated for 1 hour at

room temperature. Nuclei were stained with DAPI (catalog no R37606; Thermo Fisher Scientific) for 5 minutes at room temperature. All slides were coverslipped with mounting media (Life Technologies, Carlsbad, CA) and imaged.

Transmission Electron Microscopy

HIEs (3D) embedded in Matrigel were fixed in a solution of 2% paraformaldehyde + 2.5% glutaraldehyde + 2 mmol/L calcium chloride in 0.1 mol/L cacodylate buffer (pH = 7.4) for 5–7 days at 4°C. They were postfixed in 1% osmium tetroxide in 0.1 mol/L cacodylate buffer for 1 hour and stained en bloc with saturated aqueous uranyl acetate. After a routine dehydration sequence, tissue pieces gradually were infiltrated in a gradient series of Spurr's Low Viscosity resin (Sigma-Aldrich) and ethanol, then embedded in fresh Spurr's resin and polymerized at 60°C for 3 days. Thin sections (55–60 nm) were cut on a Leica (Wezlar, BRD) UC7 ultra-microtome using a Diatome Ultra 45 diamond knife. Sections were viewed on a Hitachi (Tokyo, Japan) H7500 transmission electron microscope set to 80 kV. Images were collected using an AMT XR-16 digital camera and AMT Image Capture (Advanced Microscopy Techniques Corp, Woburn, MA), v602.600.51 software.

Microscopy and Image Analysis

tet*NGN3*-HIEs were imaged with widefield epifluorescence on a Nikon (Tokyo, Japan) TiE inverted microscope and an upright Nikon Eclipse 90i microscope using a SPECTRA X LED light source (Lumencor, Beaverton, OR), as well as a Nikon A1plus point scanning confocal microscope for fluorescence imaging. The following objectives were used: $10\times$ Plan Fluor (numerical aperture, 0.3) phase-contrast objective, $20\times$ Plan Apo (numerical aperture, 0.75) differential interference contrast (DIC) objective, a $40\times$ Apo DIC water objective, and a Plan Apo VC $60\times$ Oil DIC objective. Fluorescence images were recorded using either an ORCA-Flash 4.0 sCMOS camera (Hamamatsu, Hamamatsu City, Japan) or a CoolSNAP HQ2 camera (Teledyne Photometrics, Tuscon, AZ), and color images for H&E sections were recorded using a DS-Fi1-U2 camera (Nikon). Nikon Elements Advanced Research v4.5 software was used for data acquisition and image analysis.

To quantify ChgA-positive cells in 3D and monolayer tet*NGN3*-HIEs, images were analyzed using Nikon Elements software. Individual images were processed with a 4-μm size threshold by channel to reduce noise from nonspecific staining. Images were separated morphologically using a 3×3 matrix, and objects touching the borders were removed. The percentage of positive cells was the number of Alexa Fluor 488–positive objects divided by the number of DAPI-stained detected nuclei. At least 5 images per condition were analyzed with an average of 140 (3D cultures) or 1400 (flat monolayers) nuclei per image.

RNA Extraction, Reverse Transcription, and Real-Time PCR

tet*NGN3*-HIEs were rinsed once with ice-cold $1\times$ PBS and transferred to a centrifugation tube (technical duplicates were combined into a single tube). Cells were lysed by the addition of 1 mL TRIzol reagent (Invitrogen) and mixed thoroughly using a vortex mixer for 30 seconds. Chloroform (200 μL) was added, the samples were mixed again, and then incubated for 5 minutes at room temperature. The phases were separated by centrifugation at $14,000 \times g$ for 10 minutes, and the aqueous phase was moved to a new tube (~ 400 μL). Total RNA then was isolated using the RNeasy Isolation Kit (Qiagen, Hilden, BRD) according to the manufacturer's instructions. RNA was eluted in 20 μL sterile nuclease free water (Thermo Fisher Scientific). RNA concentration and purity were determined by absorbance at 260 nm and 280 nm using a spectrophotometer (DS-11; DeNovix Wilmington, DE). RNA (200 ng) was treated with DNase (Ambion Turbo DNA-free Thermo Fisher Scientific) to remove any contaminating genomic DNA per the manufacturer's directions, and then complementary DNA (cDNA) was synthesized from purified total RNA using SuperScript III reverse transcriptase (Invitrogen) according to the manufacturer's instructions. Reaction components included random hexamers (Integrated DNA Technologies, Coralville, IA), 10 mmol/L deoxynucleoside triphosphate (New England BioLabs, Ipswich, MA), and approximately 2 ng of RNA. No reverse-transcriptase controls were included by omitting SuperScript III.

Real-time PCR reactions were performed in triplicate with the following reaction components: 1 μL cDNA, 0.25 μL of 20 mmol/L forward and reverse primer (Table 2), 10 μL Power SYBR Green PCR MasterMix (Applied Biosystems, Foster City, CA), and 8.5 μL nuclease-free water (Thermo Fisher Scientific). Real-time PCR was performed using QuantStudio real-time thermocycler (Applied Biosciences, Foster City, CA) under the following conditions: 95°C for 10 minutes, 40 cycles of 95°C for 15 seconds, followed by 60°C for 1 minute, when data were recorded. A melting curve between 60°C and 95°C was performed. No template controls were included by substituting water for the cDNA in the reaction. Cycle threshold values of technical replicates were averaged for each independent biological experiment and normalized to the expression of the 18S ribosomal subunit. Data graphed are representative of 3 experiments (n = 3 biological replicates, with 3 technical replicates in each experiment).

Preparation of HIE Transwells for RNA-Sequencing and Transcriptional Analysis

To assess the transcriptional profile changes of tet*NGN3*-HIEs during doxycycline induction, HIE monolayers were prepared on Transwells and differentiated as described in the Methods section "Establishment of HIE Cultures." The total RNA was extracted from Transwells in the presence or absence of 1 μg/mL doxycycline using the same protocol as for reverse-transcription and qPCR described above. Ribosomal RNA integrity was checked on an Agilent (Santa Clara, CA) 2100 bioanalyzer from 6 independent biological replicates per condition. Paired-end Illumina (San Diego, CA) sequencing was performed on mRNA-enriched samples by Novogene (Chula Vista, CA) following the standard

work-flow procedure. Raw sequence reads were mapped to human genome 19 using STAR software to generate the number of fragments per kilobase per million mapped reads for each gene. Ratios of transcript abundance per group were based on the $\log_2$ fragments per kilobase per million mapped reads value in 1 μg/mL doxycycline condition relative to the 0 μg/mL doxycycline condition were used to determine the fold change in gene expression. Samples were filtered for those containing >10% N value, presence of adaptor sequences, and quality. More than 97% of reads in each sample were clean reads postfiltering with error rates $\leq$0.03%. Pearson correlation coefficients between samples were between 0.92 and 0.97 R^2 values. In total, 10,741 genes were expressed differentially between the groups (5870 up-regulated, 4871 down-regulated) as indicated by DESeq2 analysis using a *P*adjusted value <.05, a $\log_2$ fold change >1, and a q value <0.005.

Isovalerate and Norepinephrine Stimulation

After 4 days in differentiation medium and induced with 0, 0.1, or 1 μg/mL doxycycline, confluent HIE monolayers were washed with 1$\times$ PBS. Isovalerate (Sigma-Aldrich) and noradrenaline bitartrate (Tocris Bioscience) solutions were prepared in 1$\times$ PBS and added to the HIE monolayers. Monolayers were incubated for 2 hours at 37°C and 5% CO_2. After incubation, supernatants were harvested and kept at -20°C for downstream analysis. PrestoBlue Cell Viability Reagent (ThermoFisher Scientific), a resazurin-based assay, was used according to the manufacturer's recommended protocols. Fluorescence intensity of reduced resazurin (560–610 nm, Infinite F200Pro; Tecan, Mannedorf, CHF) measures metabolic activity of the cells and was used as an indication of cell viability.

Rotavirus Infection of HIE Monolayers

African green monkey kidney (MA104) cells were cultured in DMEM supplemented with 10% (vol/vol) fetal bovine serum (Corning). Ito RV (G3[P8]) was propagated in MA104 cells in serum-free DMEM in the presence of 1 μg/mL Worthington's Trypsin (Worthington Biochemical, Lakewood, NJ). After harvest, stocks were subjected to 3 freeze/thaw cycles. Plaque assays with MA104 cells were used to determine the titers of the viral preparations. The tet*NGN3*-HIE flat or Transwell monolayers were induced with 0, 0.1, or 1 μg/mL doxycycline in differentiation media for 4–5 days. For infection, the confluent HIE monolayers were washed once with CMGF-. Mock MA104 cell lysates and Ito RV were treated with 10 μg/mL Worthington's trypsin for 30 minutes at 37°C. Then the tet*NGN3*-HIE monolayers were treated with an inoculum of CMGF- with MA104 cell lysate or Ito RV. Cells were infected basolaterally after observations that this method results in more efficient infections (Blutt et al, unpublished data). Transwell and flat monolayers were incubated for 1 or 2 hours, respectively, at 37°C with 5% CO_2. After incubation, the supernatants were removed and replaced with differentiation media and returned to the incubator. For the 1 hpi time point, supernatants were collected 5 minutes after washing inoculum. Supernatants were harvested and kept at -20°C for downstream analyses.

Measurement of Serotonin Release

Serotonin secretion by HIEs after stimulation with norepinephrine, isovalerate, or RV infection was quantified by enzyme-linked immunosorbent assay (Eagle Biosciences, Amherst, NH) according to the manufacturer's instructions. A standard curve of known serotonin concentrations was plotted against optical density at 450 nm with a limit of detection of 2.6 ng/mL (Infinite F200Pro; Tecan).

Measurement of Metabolic Hormones

Hormone secretion was quantified by Luminex assay (Human Metabolic Hormone Magnetic Bead Panel, HMHEMAG-34K; EMD Millipore) according to the manufacturer's standard protocol. After stimulation with norepinephrine or RV infection, supernatants were assayed for the amount of secreted amylin (active), C-peptide, ghrelin (active), GIP (total), GLP-1 (total), glucagon, IL6, leptin, MCP-1, PP, PYY (total), and TNF-α. Limits of detection of the assay are as follows: amylin, 11.81 pg/mL; C-peptide, 13.28 pg/mL; ghrelin, 9.40 pg/mL; GIP, 0.33 pg/mL; GLP-1, 1.11 pg/mL; glucagon, 12.73 pg/mL; IL6, 3.75 pg/mL; leptin, 54.16 pg/mL; MCP-1, 8.57 pg/mL; PP, 0.68 pg/mL; PYY, 11.18 pg/mL; and TNF-α, <0.14 pg/mL.

Statistical Analysis

Biostatistical analyses were performed using GraphPad Prism (version 7) software (GraphPad, Inc, La Jolla, CA). Comparisons were made with either 1-way or 2-way analysis of variance and the Tukey post hoc multiple comparisons test when appropriate. Differences between the groups were considered significant at $P < .05$, and the data are presented as means $\pm$ SD.

All authors had access to the study data, and reviewed and approved the final manuscript.

References

1. Ferraris RP, Lee PP, Diamond JM. Origin of regional and species differences in intestinal glucose uptake. Am J Physiol 1989;257:G689–G697.
2. Bergman EN. Energy contributions of volatile fatty acids from the gastrointestinal tract in various species. Physiol Rev 1990;70:567–590.
3. Worthington JJ, Reimann F, Gribble FM. Enteroendocrine cells-sensory sentinels of the intestinal environment and orchestrators of mucosal immunity. Mucosal Immunol 2018;11:3–20.
4. Schonhoff SE, Giel-Moloney M, Leiter AB. Minireview: development and differentiation of gut endocrine cells. Endocrinology 2004;145:2639–2644.
5. Ahlman H, Nilsson O. The gut as the largest endocrine organ in the body. Ann Oncol 2001;12(Suppl 2):S63–S68.
6. Sternini C, Anselmi L, Rozengurt E. Enteroendocrine cells: a site of 'taste' in gastrointestinal chemosensing. Curr Opin Endocrinol Diabetes Obes 2008;15:73–78.

7. Rehfeld JF. The new biology of gastrointestinal hormones. Physiol Rev 1998;78:1087–1108.

8. Sjolund K, Sanden G, Hakanson R, Sundler F. Endocrine cells in human intestine: an immunocytochemical study. Gastroenterology 1983;85:1120–1130.

9. Solcia E, Capella C, Buffa R, Usellini L, Fiocca R, Frigerio B, Tenti P, Sessa F. The diffuse endocrine-paracrine system of the gut in health and disease: ultrastructural features. Scand J Gastroenterol Suppl 1981;70:25–36.

10. Roth KA, Gordon JI. Spatial differentiation of the intestinal epithelium: analysis of enteroendocrine cells containing immunoreactive serotonin, secretin, and substance P in normal and transgenic mice. Proc Natl Acad Sci U S A 1990;87:6408–6412.

11. Andrews PL, Davis CJ, Bingham S, Davidson HI, Hawthorn J, Maskell L. The abdominal visceral innervation and the emetic reflex: pathways, pharmacology, and plasticity. Can J Physiol Pharmacol 1990; 68:325–345.

12. Hagbom M, Istrate C, Engblom D, Karlsson T, Rodriguez-Diaz J, Buesa J, Taylor JA, Loitto VM, Magnusson KE, Ahlman H, Lundgren O, Svensson L. Rotavirus stimulates release of serotonin (5-HT) from human enterochromaffin cells and activates brain structures involved in nausea and vomiting. PLoS Pathog 2011;7:e1002115.

13. Saxena K, Blutt SE, Ettayebi K, Zeng XL, Broughman JR, Crawford SE, Karandikar UC, Sastri NP, Conner ME, Opekun AR, Graham DY, Qureshi W, Sherman V, Foulke-Abel J, In J, Kovbasnjuk O, Zachos NC, Donowitz M, Estes MK. Human intestinal enteroids: a new model to study human rotavirus infection, host restriction, and pathophysiology. J Virol 2016;90:43–56.

14. Zachos NC, Kovbasnjuk O, Foulke-Abel J, In J, Blutt SE, de Jonge HR, Estes MK, Donowitz M. Human enteroids/colonoids and intestinal organoids functionally recapitulate normal intestinal physiology and pathophysiology. J Biol Chem 2016;291:3759–3766.

15. Clevers H. Modeling development and disease with organoids. Cell 2016;165:1586–1597.

16. Bartfeld S. Modeling infectious diseases and host-microbe interactions in gastrointestinal organoids. Dev Biol 2016;420:262–270.

17. Sato T, Stange DE, Ferrante M, Vries RG, Van Es JH, Van den Brink S, Van Houdt WJ, Pronk A, Van Gorp J, Siersema PD, Clevers H. Long-term expansion of epithelial organoids from human colon, adenoma, adenocarcinoma, and Barrett's epithelium. Gastroenterology 2011;141:1762–1772.

18. Sato T, Vries RG, Snippert HJ, van de Wetering M, Barker N, Stange DE, van Es JH, Abo A, Kujala P, Peters PJ, Clevers H. Single Lgr5 stem cells build crypt-villus structures in vitro without a mesenchymal niche. Nature 2009;459:262–265.

19. Foulke-Abel J, In J, Kovbasnjuk O, Zachos NC, Ettayebi K, Blutt SE, Hyser JM, Zeng XL, Crawford SE, Broughman JR, Estes MK, Donowitz M. Human enteroids as an ex-vivo model of host-pathogen interactions in the gastrointestinal tract. Exp Biol Med (Maywood) 2014;239:1124–1134.

20. Foulke-Abel J, In J, Yin J, Zachos NC, Kovbasnjuk O, Estes MK, de Jonge H, Donowitz M. Human enteroids as a model of upper small intestinal ion transport physiology and pathophysiology. Gastroenterology 2016; 150:638–649 e8.

21. Ettayebi K, Crawford SE, Murakami K, Broughman JR, Karandikar U, Tenge VR, Neill FH, Blutt SE, Zeng XL, Qu L, Kou B, Opekun AR, Burrin D, Graham DY, Ramani S, Atmar RL, Estes MK. Replication of human noroviruses in stem cell-derived human enteroids. Science 2016;353:1387–1393.

22. Apelqvist A, Li H, Sommer L, Beatus P, Anderson DJ, Honjo T, Hrabe de Angelis M, Lendahl U, Edlund H. Notch signalling controls pancreatic cell differentiation. Nature 1999;400:877–881.

23. Gradwohl G, Dierich A, LeMeur M, Guillemot F. neurogenin3 is required for the development of the four endocrine cell lineages of the pancreas. Proc Natl Acad Sci U S A 2000;97:1607–1611.

24. Jenny M, Uhl C, Roche C, Duluc I, Guillermin V, Guillemot F, Jensen J, Kedinger M, Gradwohl G. Neurogenin3 is differentially required for endocrine cell fate specification in the intestinal and gastric epithelium. EMBO J 2002;21:6338–6347.

25. Jensen J, Heller RS, Funder-Nielsen T, Pedersen EE, Lindsell C, Weinmaster G, Madsen OD, Serup P. Independent development of pancreatic alpha- and beta-cells from neurogenin3-expressing precursors: a role for the notch pathway in repression of premature differentiation. Diabetes 2000;49:163–176.

26. Schwitzgebel VM, Scheel DW, Conners JR, Kalamaras J, Lee JE, Anderson DJ, Sussel L, Johnson JD, German MS. Expression of neurogenin3 reveals an islet cell precursor population in the pancreas. Development 2000;127:3533–3542.

27. Suissa Y, Magenheim J, Stolovich-Rain M, Hija A, Collombat P, Mansouri A, Sussel L, Sosa-Pineda B, McCracken K, Wells JM, Heller RS, Dor Y, Glaser B. Gastrin: a distinct fate of neurogenin3 positive progenitor cells in the embryonic pancreas. PLoS One 2013;8:e70397.

28. McGrath PS, Watson CL, Ingram C, Helmrath MA, Wells JM. The basic helix-loop-helix transcription factor NEUROG3 is required for development of the human endocrine pancreas. Diabetes 2015;64:2497–2505.

29. Spence JR, Mayhew CN, Rankin SA, Kuhar MF, Vallance JE, Tolle K, Hoskins EE, Kalinichenko VV, Wells SI, Zorn AM, Shroyer NF, Wells JM. Directed differentiation of human pluripotent stem cells into intestinal tissue in vitro. Nature 2011;470:105–109.

30. Sinagoga KL, Wells JM. Generating human intestinal tissues from pluripotent stem cells to study development and disease. EMBO J 2015;34:1149–1163.

31. Pinney SE, Oliver-Krasinski J, Ernst L, Hughes N, Patel P, Stoffers DA, Russo P, De Leon DD. Neonatal diabetes and congenital malabsorptive diarrhea attributable to a novel mutation in the human neurogenin-3 gene coding sequence. J Clin Endocrinol Metab 2011; 96:1960–1965.

32. Rubio-Cabezas O, Jensen JN, Hodgson MI, Codner E, Ellard S, Serup P, Hattersley AT. Permanent neonatal

diabetes and enteric anendocrinosis associated with biallelic mutations in NEUROG3. Diabetes 2011; 60:1349–1353.

33. German-Diaz M, Rodriguez-Gil Y, Cruz-Rojo J, Charbit-Henrion F, Cerf-Bensussan N, Manzanares-Lopez Manzanares J, Moreno-Villares JM. A new case of congenital malabsorptive diarrhea and diabetes secondary to mutant neurogenin-3. Pediatrics 2017; 140:e1–e6.

34. Jensen JN, Rosenberg LC, Hecksher-Sorensen J, Serup P. Mutant neurogenin-3 in congenital malabsorptive diarrhea. N Engl J Med 2007; 356:1781–1782.

35. Unlusoy Aksu A, Egritas Gurkan O, Sari S, Demirtas Z, Turkyilmaz C, Poyraz A, Dalgic B. Mutant neurogenin-3 in a Turkish boy with congenital malabsorptive diarrhea. Pediatr Int 2016;58:379–382.

36. Wang J, Cortina G, Wu SV, Tran R, Cho JH, Tsai MJ, Bailey TJ, Jamrich M, Ament ME, Treem WR, Hill ID, Vargas JH, Gershman G, Farmer DG, Reyen L, Martin MG. Mutant neurogenin-3 in congenital malabsorptive diarrhea. N Engl J Med 2006;355:270–280.

37. Ueo T, Imayoshi I, Kobayashi T, Ohtsuka T, Seno H, Nakase H, Chiba T, Kageyama R. The role of Hes genes in intestinal development, homeostasis and tumor formation. Development 2012;139:1071–1082.

38. Chen YJ, Finkbeiner SR, Weinblatt D, Emmett MJ, Tameire F, Yousefi M, Yang C, Maehr R, Zhou Q, Shemer R, Dor Y, Li C, Spence JR, Stanger BZ. De novo formation of insulin-producing "neo-beta cell islets" from intestinal crypts. Cell Rep 2014;6:1046–1058.

39. Ootani A, Li X, Sangiorgi E, Ho QT, Ueno H, Toda S, Sugihara H, Fujimoto K, Weissman IL, Capecchi MR, Kuo CJ. Sustained in vitro intestinal epithelial culture within a Wnt-dependent stem cell niche. Nat Med 2009; 15:701–706.

40. Sinagoga KL, McCauley HA, Munera JO, Reynolds NA, Enriquez JR, Watson C, Yang HC, Helmrath MA, Wells JM. Deriving functional human enteroendocrine cells from pluripotent stem cells. Development 2018:145.

41. McCracken KW, Aihara E, Martin B, Crawford CM, Broda T, Treguier J, Zhang X, Shannon JM, Montrose MH, Wells JM. Wnt/beta-catenin promotes gastric fundus specification in mice and humans. Nature 2017;541:182–187.

42. Perry JL, Ramachandran NK, Utama B, Hyser JM. Use of genetically-encoded calcium indicators for live cell calcium imaging and localization in virus-infected cells. Methods 2015;90:28–38.

43. Wade PR, Westfall JA. Ultrastructure of enterochromaffin cells and associated neural and vascular elements in the mouse duodenum. Cell Tissue Res 1985; 241:557–563.

44. VanDussen KL, Marinshaw JM, Shaikh N, Miyoshi H, Moon C, Tarr PI, Ciorba MA, Stappenbeck TS. Development of an enhanced human gastrointestinal epithelial culture system to facilitate patient-based assays. Gut 2015;64:911–920.

45. Leushacke M, Barker N, Pin C. Quantifying Lgr5-positive stem cell behaviour in the pyloric epithelium. Sci Rep 2016;6:21923.

46. Bertrand PP, Barajas-Espinosa A, Neshat S, Bertrand RL, Lomax AE. Analysis of real-time serotonin (5-HT) availability during experimental colitis in mouse. Am J Physiol Gastrointest Liver Physiol 2010; 298:G446–G455.

47. Linden DR, Foley KF, McQuoid C, Simpson J, Sharkey KA, Mawe GM. Serotonin transporter function and expression are reduced in mice with TNBS-induced colitis. Neurogastroenterol Motil 2005;17:565–574.

48. Wheatcroft J, Wakelin D, Smith A, Mahoney CR, Mawe G, Spiller R. Enterochromaffin cell hyperplasia and decreased serotonin transporter in a mouse model of postinfectious bowel dysfunction. Neurogastroenterol Motil 2005;17:863–870.

49. Bischoff SC, Mailer R, Pabst O, Weier G, Sedlik W, Li Z, Chen JJ, Murphy DL, Gershon MD. Role of serotonin in intestinal inflammation: knockout of serotonin reuptake transporter exacerbates 2,4,6-trinitrobenzene sulfonic acid colitis in mice. Am J Physiol Gastrointest Liver Physiol 2009;296:G685–G695.

50. Coates MD, Mahoney CR, Linden DR, Sampson JE, Chen J, Blaszyk H, Crowell MD, Sharkey KA, Gershon MD, Mawe GM, Moses PL. Molecular defects in mucosal serotonin content and decreased serotonin reuptake transporter in ulcerative colitis and irritable bowel syndrome. Gastroenterology 2004;126:1657–1664.

51. Khan WI. The role of 5-HT dysregulation in inflammatory bowel disease. Gastroenterol Hepatol (N Y) 2013; 9:259–261.

52. Wang Y, Gong H, Lopez R, Lian L, Kiran RP, Soffer EE, Shen B. Correlation between serum serotonin and endoscopy inflammation scores in patients with ileal pouches. J Crohns Colitis 2013;7:e133–e142.

53. Thomson AB, Drozdowski L, Iordache C, Thomson BK, Vermeire S, Clandinin MT, Wild G. Small bowel review: normal physiology, part 2. Dig Dis Sci 2003; 48:1565–1581.

54. Bellono NW, Bayrer JR, Leitch DB, Castro J, Zhang C, O'Donnell TA, Brierley SM, Ingraham HA, Julius D. Enterochromaffin cells are gut chemosensors that couple to sensory neural pathways. Cell 2017; 170:185–198 e16.

55. Bialowas S, Hagbom M, Nordgren J, Karlsson T, Sharma S, Magnusson KE, Svensson L. Rotavirus and serotonin cross-talk in diarrhoea. PLoS One 2016; 11:e0159660.

56. Gabanyi I, Muller PA, Feighery L, Oliveira TY, Costa-Pinto FA, Mucida D. Neuro-immune interactions drive tissue programming in intestinal macrophages. Cell 2016;164:378–391.

57. Neis EP, Dejong CH, Rensen SS. The role of microbial amino acid metabolism in host metabolism. Nutrients 2015;7:2930–2946.

58. Cox HM. Neuropeptide Y receptors; antisecretory control of intestinal epithelial function. Auton Neurosci 2007; 133:76–85.

59. O'Mahony SM, Clarke G, Borre YE, Dinan TG, Cryan JF. Serotonin, tryptophan metabolism and the brain-gut-microbiome axis. Behav Brain Res 2015;277:32–48.

60. Yano JM, Yu K, Donaldson GP, Shastri GG, Ann P, Ma L, Nagler CR, Ismagilov RF, Mazmanian SK, Hsiao EY. Indigenous bacteria from the gut microbiota regulate host serotonin biosynthesis. Cell 2015;161:264–276.

61. Evrensel A, Ceylan ME. The gut-brain axis: the missing link in depression. Clin Psychopharmacol Neurosci 2015; 13:239–244.

62. Tsuruta T, Saito S, Osaki Y, Hamada A, Aoki-Yoshida A, Sonoyama K. Organoids as an ex vivo model for study-ing the serotonin system in the murine small intestine and colon epithelium. Biochem Biophys Res Commun 2016;474:161–167.

63. Kishida K, Pearce SC, Yu S, Gao N, Ferraris RP. Nutrient sensing by absorptive and secretory progenies of small intestinal stem cells. Am J Physiol Gastrointest Liver Physiol 2017;312:G592–G605.

64. McCracken KW, Cata EM, Crawford CM, Sinagoga KL, Schumacher M, Rockich BE, Tsai YH, Mayhew CN, Spence JR, Zavros Y, Wells JM. Modelling human development and disease in plurip-otent stem-cell-derived gastric organoids. Nature 2014;516:400–404.

65. Dekkers JF, Berkers G, Kruisselbrink E, Vonk A, de Jonge HR, Janssens HM, Bronsveld I, van de Graaf EA, Nieuwenhuis EE, Houwen RH, Vleggaar FP, Escher JC, de Rijke YB, Majoor CJ, Heijerman HG, de Winter-de Groot KM, Clevers H, van der Ent CK, Beekman JM. Characterizing responses to CFTR-modulating drugs using rectal organoids derived from subjects with cystic fibrosis. Sci Transl Med 2016;8:344ra84.

66. Rollo EE, Kumar KP, Reich NC, Cohen J, Angel J, Greenberg HB, Sheth R, Anderson J, Oh B, Hempson SJ, Mackow ER, Shaw RD. The epithelial cell response to rotavirus infection. J Immunol 1999; 163:4442–4452.

67. Basak O, Beumer J, Wiebrands K, Seno H, van Oudenaarden A, Clevers H. Induced quiescence of Lgr5+ stem cells in intestinal organoids enables differ-entiation of hormone-producing enteroendocrine cells. Cell Stem Cell 2017;20:177–190 e4.

68. Grun D, Lyubimova A, Kester L, Wiebrands K, Basak O, Sasaki N, Clevers H, van Oudenaarden A. Single-cell messenger RNA sequencing reveals rare intestinal cell types. Nature 2015;525:251–255.

69. Petersen N, Reimann F, Bartfeld S, Farin HF, Ringnalda FC, Vries RG, van den Brink S, Clevers H, Gribble FM, de Koning EJ. Generation of L cells in mouse and human small intestine organoids. Diabetes 2014; 63:410–420.

70. Zietek T, Rath E, Haller D, Daniel H. Intestinal organoids for assessing nutrient transport, sensing and incretin secretion. Sci Rep 2015;5:16831.

71. Petersen N, Reimann F, van Es JH, van den Berg BM, Kroone C, Pais R, Jansen E, Clevers H, Gribble FM, de Koning EJ. Targeting development of incretin-producing cells increases insulin secretion. J Clin Invest 2015; 125:379–385.

72. Bohorquez DV, Samsa LA, Roholt A, Medicetty S, Chandra R, Liddle RA. An enteroendocrine cell-enteric glia connection revealed by 3D electron microscopy. PLoS One 2014;9:e89881.

73. Pattison AM, Blomain ES, Merlino DJ, Wang F, Crissey MA, Kraft CL, Rappaport JA, Snook AE, Lynch JP, Waldman SA. Intestinal enteroids model guanylate cyclase C-dependent secretion induced by heat-stable enterotoxins. Infect Immun 2016; 84:3083–3091.

74. Criglar JM, Hu L, Crawford SE, Hyser JM, Broughman JR, Prasad BV, Estes MK. A novel form of rotavirus NSP2 and phosphorylation-dependent NSP2-NSP5 interactions are associated with viroplasm as-sembly. J Virol 2014;88:786–798.

75. Castro I, Aguilera S, Brockhausen I, Alliende C, Quest AF, Molina C, Urzua U, Mandel U, Bahamondes V, Barrera MJ, Sanchez M, Gonzalez S, Hermoso M, Leyton C, Gonzalez MJ. Decreased salivary sulpho-transferase activity correlated with inflammation and autoimmunity parameters in Sjogren's syndrome pa-tients. Rheumatology (Oxford) 2012;51:482–490.

76. Andreu P, Peignon G, Slomianny C, Taketo MM, Colnot S, Robine S, Lamarque D, Laurent-Puig P, Perret C, Romagnolo B. A genetic study of the role of the Wnt/beta-catenin signalling in Paneth cell differentiation. Dev Biol 2008;324:288–296.

77. Papetti M, Augenlicht LH. MYBL2, a link between pro-liferation and differentiation in maturing colon epithelial cells. J Cell Physiol 2011;226:785–791.

78. Gaudier E, Jarry A, Blottiere HM, de Coppet P, Buisine MP, Aubert JP, Laboisse C, Cherbut C, Hoebler C. Butyrate specifically modulates MUC gene expression in intestinal epithelial goblet cells deprived of glucose. Am J Physiol Gastrointest Liver Physiol 2004; 287:G1168–G1174.

79. Adnan H, Quach H, MacIntosh K, Antenos M, Kirby GM. Low levels of GSTA1 expression are required for Caco-2 cell proliferation. PLoS One 2012;7:e51739.

80. Radek KA, Lopez-Garcia B, Hupe M, Niesman IR, Elias PM, Taupenot L, Mahata SK, O'Connor DT, Gallo RL. The neuroendocrine peptide catestatin is a cutaneous antimicrobial and induced in the skin after injury. J Invest Dermatol 2008;128:1525–1534.

81. Croitoru-Lamoury J, Lamoury FM, Caristo M, Suzuki K, Walker D, Takikawa O, Taylor R, Brew BJ. Interferon-gamma regulates the proliferation and differentiation of mesenchymal stem cells via activation of indoleamine 2, 3 dioxygenase (IDO). PLoS One 2011;6:e14698.

Correspondence
Address correspondence to: Joseph M. Hyser, PhD, or Robert A. Britton, PhD, Alkek Center for Metagenomics and Microbiome Research, Department of Molecular Virology and Microbiology, Baylor College of Medicine, One Baylor Plaza, MS: BCM385, Houston, Texas. e-mail: Joseph.hyser@bcm.edu or Robert.Britton@bcm.edu; fax: (713) 798-3586.

Author contributions

Alexandra L. Chang-Graham, Heather A. Danhof, Melinda A. Engevik, Catherine Tomaro-Duchesneau, Umesh C. Karandikar, Mary K. Estes, Robert A. Britton, and Joseph M. Hyser were responsible for the concept and design; Alexandra L. Chang-Graham, Heather A. Danhof, Melinda A. Engevik, Catherine Tomaro-Duchesneau, Umesh C. Karandikar, Mary K. Estes, James Versalovic, Robert A. Britton, and Joseph M. Hyser provided intellectual contributions; Alexandra L. Chang-Graham, Heather A. Danhof, Melinda A. Engevik, Catherine Tomaro-Duchesneau, and Umesh C. Karandikar acquired data; Alexandra L. Chang-Graham, Heather A. Danhof, Melinda A. Engevik, Catherine Tomaro-Duchesneau, and Umesh C. Karandikar performed the data analysis, statistical analysis, and interpretation; Alexandra L. Chang-Graham, Heather A. Danhof, Melinda A. Engevik, and Joseph M. Hyser drafted and edited the manuscript; and Mary K. Estes, James Versalovic, Robert A. Britton, and Joseph M. Hyser obtained funding.

Conflicts of interest

The authors disclose no conflicts.